

Radar Detection of a drone using a S-Band Radar



Prepared by:
Nyasha Mashanda
MSHNYA010
Department of Electrical Engineering
University of Cape Town

Prepared for:
Dr Yunus Abdul Gaffar & Dr Francois Schonken
DEPARTMENT OF ELECTRICAL ENGINEERING
University of Cape Town

October 2019

Submitted to the Department of Electrical Engineering at the University of Cape Town in partial fulfilment of the academic requirements for a Bachelor of Science degree in Electrical Engineering.

Declaration

1. I know that plagiarism is wrong. Plagiarism is to use another's work and pretend that it is one's own.
2. I have used the IEEE convention for citation and referencing. Each contribution to, and quotation in, this final year project report from the work(s) of other people, has been attributed and has been cited and referenced.
3. This final year project report is my own work.
4. I have not allowed, and will not allow, anyone to copy my work with the intention of passing it off as their own work or part thereof

Name: NYASHA MASHANDA

Signature: N.M Date: 15 October 2019

Terms of Reference

It was agreed that the following deliverables be achieved for the completion of the project:

- Understand Frequency modulated Continuous Wave radar theory and construct an S-Band radar based on the MIT documentation
- Review what has been done by other researchers to solve the problem of drone detection
- Development of a Graphical User Interface to record and process data. It is important to note that this was done by an electrical engineering student as part of their work hence this was removed from the scope of the project
- Package the radar in a robust manner, powered by a battery source at least for 4 hours
- Perform various experiments with careful planning and execution for the detection of drones
- Apply signal processing techniques to detect drones and quantify the performance of the system

Acknowledgements

I would like to acknowledge the following people for their assistance and support in the course of the project.

Dr. Yunus Abdul Gaffar, my advisor, for ensuring that the whole learning experience was interestingly challenging. This was achieved by motivating me to explore the world of radar and at other times, teaching the concepts behind radar. Furthermore, his time management skills inspired me to grow in the same area. Thank you!

Dr. Francois Schonken for being a dependable advisor when Dr Yunus was not available. Additionally, his expertise was useful in certain parts of the project.

Wian Van Zyl for providing a drone that we used for carrying out experiments. He was willing to spare his valuable time to help undertake the experiments.

Ferial Najaar and Mueez Allie for assisting in carrying out drone experiments.

And finally, my wonderful parents, who supported me all the way. They have always believed in me more than I believe in myself!

Abstract

The report will cover three main tasks that were completed in 12 weeks.

The first task was to build an FMCW/CW S-Band radar from the plans provided by the MIT IAP Radar course. This is best done with a good understanding of the relevant theory behind radar systems. Therefore, the report will include radar theory before going into detail on the processes followed to build the radar.

The second task was to understand the principles behind detection algorithms. This entailed looking at various CFARs', attempting to investigate their respective strengths and weaknesses.

The third task was to carry out various experiments to detect moving drones. After collecting the results from the experiments, various CFAR algorithms were applied on the data and their performance compared to find the best CFAR for drone detection. In the end the it was decided to pick one CFAR based on additional advantages.

The results suggested that it is possible to detect small drones using an S-Band radar.

All the code produced for this report can be found at this link:

<https://drive.google.com/drive/folders/1fvdmTBGShr0pXFkTisCqXJGrcRPA4wkn?usp=sharing>

Table of Contents

Declaration	i
Terms of Reference	ii
Acknowledgements	iii
Abstract.....	iv
Table of Contents	v
List of tables	xi
1 Introduction.....	1
1.1 Background to the study	1
1.2 Objectives of this study	2
Problems Statement	2
Objectives	2
1.3 Scope and Limitations	2
1.4 Plan of Development	3
2 Literature Review	4
3 Radar Theory	8
3.1 Antenna theory.....	8
3.2 CW and FMCW Theory	9
Continuous Wave (CW) Radar.....	9
Frequency Modulated Continuous Wave (FMCW)	11
3.3 Radar Construction	14
Antennas	14
High-frequency circuit	19
Low-frequency circuit	21
Active low pass filter circuit.....	23
Signal generator circuit	25
PCB Design.....	27
Base and Assembly.....	29
Testing the radar.....	29
4 Detection Theory.....	32
4.1 Linear and Square Law Rectifiers.....	32
Linear law rectifier	32
Square law rectifier.....	32
4.2 Threshold Detection of Radar Targets	32
4.3 Detectors.....	33
Neyman-Pearson Detector.....	33

CFAR Detectors	34
The Cell-Averaging CFAR (CACFAR)	34
GO-CA-CFAR.....	37
Smallest-Of CACFAR (SOCACFAR).....	38
OS-CFAR	39
TM-CFAR.....	40
5 Implementation of CFAR	42
5.1 CACFAR	42
Implementation	42
Verification	42
5.2 SOCACFAR	43
Implementation	43
Verification	43
5.3 GOCACFAR	44
Implementation	44
Verification	44
5.4 OSCFAR	44
Implementation	44
Verification	45
6 Experiments and Results	46
6.1 Equipment	46
6.2 Drone hazards.....	47
6.3 Clutter Modelling	47
6.4 Radar Cross Section	47
6.5 MTI filtering.....	48
6.6 Initial experiments and improvements	49
Experiment 1	51
Experiment 2	52
Experiment 3	54
7 CFAR Results	56
7.1 Range Detection	56
7.2 Probability of detection calculation.....	58
7.3 Result 1.....	60
Results summary	60
7.4 Result 2.....	61
Result Summary	61
7.5 Result 3.....	62
Result Summary	62
8 Analysis of results.....	63

8.1	S-Band Radar Design	63
8.2	Probability of Detection	63
9	Conclusions and Recommendations.....	65
9.1	Conclusions	65
9.2	Recommendations	65
10	References.....	67
11	Appendices	69
12	EBE Faculty: Assessment of Ethics in Research Projects.....	76

List of Figures

Figure 1: Range-Doppler plot results	5
Figure 2: Maximum detectable range- Transmission power plot	5
Figure 3: Joint range and cross-range trajectory in tracking mode	5
Figure 4: Range Trajectory	6
Figure 5: Micro-doppler signature of a flying drone.....	6
Figure 6: 1-d range profile of targets.....	7
Figure 7: Results of A-CFAR aiming at drones.....	7
Figure 8: Circuit realisation of a CW radar.....	10
Figure 9: Circuit realisation of FMCW radar	11
Figure 10: Stationary drone frequency readings.....	12
Figure 11: Moving drone frequency readings	13
Figure 12: Solid works diagram of the antenna (mm)	16
Figure 13: Flange Mount SMA Connector. Adapted from [10].....	17
Figure 14: Interior of the antenna.....	17
Figure 15: Exterior of the antenna.....	17
Figure 16: Antenna testing equipment.....	18
Figure 17: Antenna S11 before tuning	18
Figure 18: Antenna S11 after tuning.....	19
Figure 19: High-frequency circuit.....	20
Figure 20: High-frequency circuit implemented	20
Figure 21: Low-frequency circuit. Adapted from [3]	21
Figure 22: Breadboard circuit	22
Figure 23: Voltage regulator results.....	22
Figure 24: Gain circuit results.....	24
Figure 25: Filtering circuit results.....	24
Figure 26: Signal generator circuit. Adapted from [3].....	25
Figure 27: Excerpt of Minicircuits VCO. Adapted from [11]	26
Figure 28: Signal generator circuit results	26
Figure 29: PCB schematic.....	27
Figure 30: PCB before being populated	28
Figure 31: PCB after population by components.....	28
Figure 32: Radar before enclosing	29
Figure 33: Radar after enclosing	29
Figure 34: Person walking away from the radar (range detection).....	30
Figure 35: Person walking away and then towards the radar (range detection)	30

Figure 36: Person walking away from the radar (speed detection).....	31
Figure 37: Person walking away and then towards the radar (speed detection)	31
Figure 38: Basic implementation of CFAR algorithms	34
Figure 39: CACFAR without guard cells. Adapted from [12]	36
Figure 40: CACFAR after applying guard cells. Adapted from [12].....	36
Figure 41: Clutter boundary	37
Figure 42: CACFAR and GOCACFAR on clutter edges [12]	38
Figure 43: CACFAR Pd results	42
Figure 44: SOCACFAR Pd results	43
Figure 45: GOCACFAR Pd results	44
Figure 46: OSCFAR Pd results.....	45
Figure 47: GUI interface	46
Figure 48: RTI map before MTI	48
Figure 49: RTI map after MTI	48
Figure 50: Front section of a drone [19]	49
Figure 51: Side section of a drone [19]	49
Figure 52: RTI map with drone front section	49
Figure 53: RTI map with a drone side section.....	50
Figure 54: RTI map with a drone at a height of 1.5 above the radar with the radar at an angle.....	50
Figure 55: Corner reflector before applying aluminium foil	50
Figure 56: Corner reflector after applying aluminium foil	51
Figure 57: RTI map results with corner reflector	51
Figure 58: Sports Centre setup	52
Figure 59: Noise only (no target)	52
Figure 60: Drone moving away	52
Figure 61: Noise only.....	53
Figure 62: Drone moving away	53
Figure 63: Drone moving away and then towards	53
Figure 64: Drone moving towards and then away	54
Figure 65: Cricket field setup	54
Figure 66: Noise only.....	55
Figure 67: Drone moving towards	55
Figure 68: Drone moving away	55
Figure 69: Final results from experiment 1	56
Figure 70: Final results from experiment 2.1	57
Figure 71: Final results from experiment 2.2	57
Figure 72: Final results from experiment 2.3	57
Figure 73: Final results from experiment 3.1	58

Figure 74: Final results from experiment 3.2	58
Figure 75: Picture showing a maximum target extent of 9 cells and missed detections	59
Figure 76: Drone moving away and towards.....	69
Figure 77: Drone moving away slowly	69
Figure 78: drone flying towards and away.....	70
Figure 79: Drone flying cross range.....	70
Figure 80: Drone flying away slowly	71
Figure 81: Drone flying towards.....	71
Figure 82: Drone flying away and then towards	72
Figure 83: Drone flying towards.....	72
Figure 84: Drone flying towards.....	72
Figure 85: Drone flying cross range.....	73
Figure 86: Drone flying cross range.....	73
Figure 87: Drone flying towards.....	73
Figure 88: Drone flying away and towards	74
Figure 89: Drone flying away and towards	74
Figure 90: Drone flying away and towards	75
Figure 91: Drone flying away and towards	75
Figure 92: Drone flying towards.....	75

List of tables

Table 1: Different velocity ranges of moving targets	7
Table 2: High-frequency parts and their part number	20
Table 3: Drone specifications	46
Table 4: Showing new experiment name.....	59
Table 5: Experiment results N = 16	60
Table 6: Graphic results N = 16	60
Table 7: Results N = 32.....	61
Table 8: Graphic results N = 32	61
Table 9: Experiment results N = 48	62
Table 10: Graphic results N = 48	62

1 Introduction

1.1 Background to the study

The use of high-frequency radio signals to detect objects, either moving or stationary, has become widespread over the past decades. Systems that use this technology are formally known as Radio Detection and Ranging (RADAR) systems. These systems have been used to find the position and velocity of objects like cars, ships at sea and aeroplanes.

Unmanned Aerial Vehicles (UAV) or drones, have become part of the list of targets of interest. In the past decade, drones have become smaller, cheaper and easier to use. As a result, drones are no longer reserved for military use as they are now accessible to civilians and industries. People have benefited from using drones for various purposes like filming, inspecting powerlines, surveying land and locating survivors during disasters. However, the widespread use of drones has led to a rise in threats like security breaches, collision with civil and military planes and terrorist attacks since drones can easily penetrate the highest levels of security.

In September 2019, Saudi Aramco, one of the largest oil-producing companies, was bombed by terrorist drones, and this resulted in 5% of the global supply of being disabled [1]. This is just one of the many incidences [2] that have been reported over the past years. To prevent the threats that come with drones, there is a need for highly accurate detection systems that can detect drones under different environmental conditions, so that interception measures can be taken if necessary.

This report will focus on the detection of a drone using radar and the aim is to find algorithms that will facilitate the detection with high accuracy. This aim will be achieved by building an S-Band (2.4-2.5 GHz) radar and then running multiple experiments to collect detection data. Various algorithms will then be applied to find the probability of detection and the results will be compared.

The results of this project might show which algorithms perform better than other when it comes to detecting drones, and this information can be used to select algorithms under specific environmental conditions.

1.2 Objectives of this study

Problems Statement

Compared to other air targets, drones are much more difficult to detect because of their size, slow movement and low altitude. As a result, returns from a drone have to compete with high clutter signals. This report aims to identify the best algorithm for drone detection within a specified range.

Objectives

This study will focus on the building of an FMCW/CW S-Band radar and the detection algorithms used for decision making in radar systems. Therefore, the following objectives are to be met

1. Understand FMCW and CW modes of operation for radars and relevant radar theory on range detection
2. Construct a working S-Band FMCW/CW Radar, based on the plans provided by the MIT IAP radar course [3].
3. Investigate different detection algorithms that can be used for drone detection
4. Perform experiments to detect drones in different environments and apply different algorithms on the results
5. Identify the algorithm that will maximise the probability of detection within a specified range
6. Give conclusions and recommendations for further investigations

1.3 Scope and Limitations

The scope of this research project includes:

- Radar theory necessary to build an FMCW/CW radar with a reasonable understanding of the purpose of each section/component and the steps taken in making the radar
- Radar detection theory necessary to understand the basic principles behind detection algorithms and their accompanying strengths and weaknesses
- Range detection of moving targets
- MATLAB code used to calculate the probability of detection within a specified range

The scope of this research does not include:

- Doppler measurements for identifying the speed of moving targets
- Design of a new detection algorithm

- Classification and tracking of targets

The study will be limited by:

- The type of radar used for detecting drones (S-band radar based on MIT documentation design). This will define the operating frequency regions of the drone
- The number of drones available for experimental procedures (1)
- The time allocated for this project (12 weeks)
- The budget allocated for the project (R1500)
- The environments accessible for doing drone experiments

1.4 Plan of Development

This report adheres to the following plan of development

- Chapter 2 will focus on the **Literature Review**, which contains information on what has been done by other researchers towards the detection of drones.
- Chapter 3 will focus on the relevant **Radar Theory** necessary to understand how an FMCW radar operates and then the construction of an S-Band FMCW/CW radar
- Chapter 4 then looks at the **Detection Theory**. Traditional detection algorithms will be looked at in greater detail to understand how, why and when to apply the algorithms
- Chapter 5 focuses on **Testing** the implementation of CFAR algorithms
- Chapter 6 looks at the field **Experiments and Results** from the experiments
- Chapter 7 will focus on applying detection algorithms to get **CFAR Results**
- Chapter 8 will then look at the **Analysis of Results**
- Chapter 9 focuses on the **Conclusion** reached and **Recommendations**

2 Literature Review

This literature review will serve the following purposes:

- Inform the reader on the methods that have been applied by other researchers towards the detection of drones
- Identify any associated advantages or disadvantages of these methods
- Find the principal results and conclusions reached
- Identify what missing information

Detection of drones is a matter of high priority, given the events that have occurred. Several methods have been proposed for detection, and these include exploiting sound waves produced by the rotating blades of the propellers [4] and using cameras for detection [5]. However, such systems face problems under unfavourable conditions for example, in noisy environments which reduces audibility, or in smoke or darkness that prevent optical sensor operations. Under such circumstances, RADAR is an effective way of detecting drones as it can work effectively in both environments.

Martins et al. have contributed to the research of drone detection by using a 24 GHz FMCW radar with a bandwidth of 500 MHz to collect results [6]. In the study, a DJI Phantom 4 Pro drone was used in the experiments, and the aim was to identify the position and velocity of a flying drone. The research also investigated the relationship between the radar cross-section (RCS) of target objects and their maximum detectable range. In taking measurements, the clutter statistics were modelled by a Weibull distribution before applying CACFAR for making detection decisions. Furthermore, micro-doppler results were collected for target classification purposes.

The results showed that CACFAR was capable of making correct drone detection decisions. Additionally, results from the RCS experiments showed that there is a strong relationship between an object's RCS and its maximum detectable range. Hence, the maximum detectable range of the drone will be lower compared to other targets that have a bigger RCS like humans and automobiles. The unique micro-doppler signature of the drone was clear enough to be distinguished from that of a walking human. However, in the research, there was no explanation given why CACFAR was chosen as the detection algorithm. The results from the experiment are as follows:

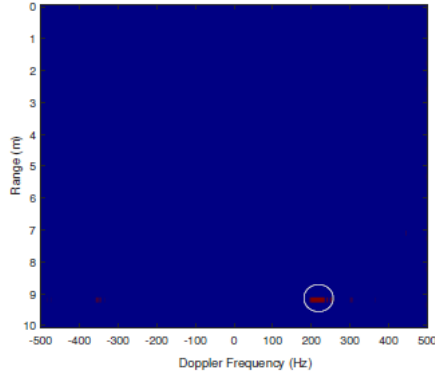


Figure 1: Range-Doppler plot results

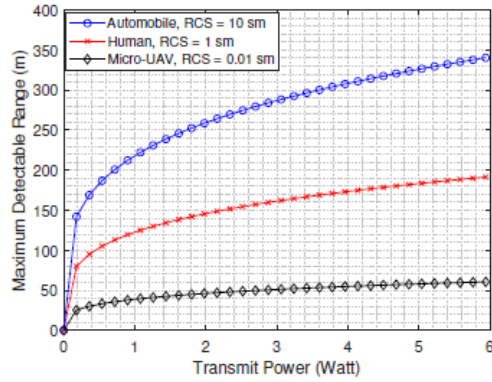


Figure 2: Maximum detectable range- Transmission power plot

Jian et al. in [7] addressed the problem of drone detection by using a Phase-Interferometric FMCW/CW Dopper Radar at 5.8 GHz with a bandwidth of 500 MHz. Using two receiving channels, phase interferometry principles together with CFAR based range-doppler processing, the range, velocity and angle of approach of a drone was determined. The results suggested that drone tracking was possible since information on the angle of approach could be obtained. The range-time map in Fig. 4 confirmed the tracking results to be correct.

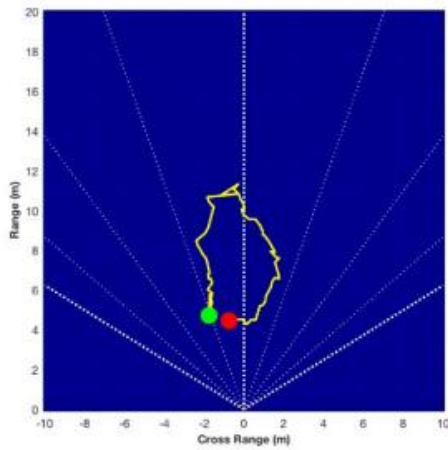


Figure 3: Joint range and cross-range trajectory in tracking mode

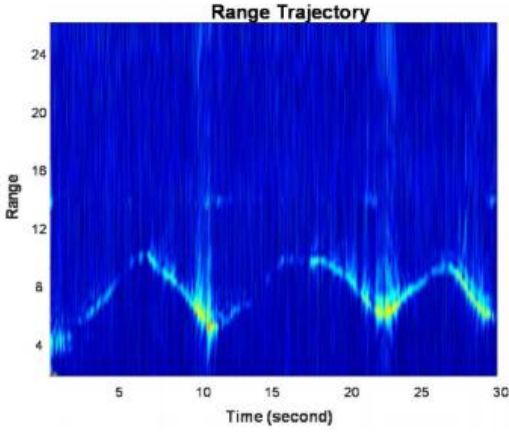


Figure 4: Range Trajectory

Furthermore, Jian et al. were able to collect the following micro-doppler results of the drone.

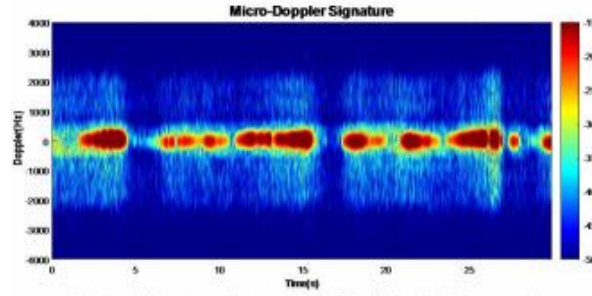


Figure 5: Micro-doppler signature of a flying drone

Unfortunately, the paper failed to mention the specific CFAR algorithm used to tackle the detection problem.

Yang et al. proposed a passive radar array system that uses Orthogonal Frequency Division Multiplexing (OFDM) echoes of drones for signal processing [8]. The detection algorithm used, A-CFAR, was a combination of CACFAR, GOCFAR and SOCACFAR. This was done to utilise the advantages that come with each CFAR. A-CFAR had an averaging unit, subtracting unit and minima determining unit. The threshold of A-CFAR was lower compared to the threshold of each individual CFARs' and as a result, there were many false alarms in the system.

An experiment was carried out with 3 drones at different radial distances from the antennas (2 750 m, 2 800m and 2 830m). The following results were collected:

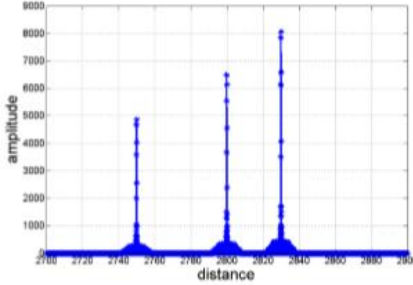


Figure 6: 1-d range profile of targets

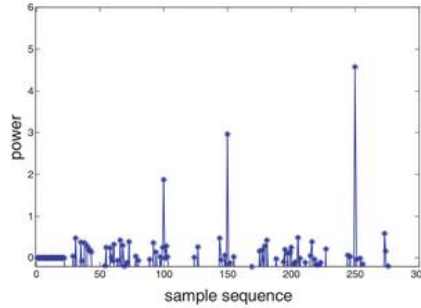


Figure 7: Results of A-CFAR aiming at drones

Fig. 7 shows the target returns combined with numerous false detections. To validate the detection of a drone, judgement by radial velocity was used to confirm if the detection made was a drone. This was possible because various targets move at different ranges of velocities. The following table of velocity ranges used to distinguish drones from other targets that created false alarms in the system.

Table 1: Different velocity ranges of moving targets

Target	Velocity range(m/s)
Low-speed bird	[8, 10]
High-speed bird	[200, 400]
UAV	[70, 120]
Fire balloon	[5, 10]
Parachute	[6, 20]
Kite	[0, 4]

The solution proposed is however not sufficient. For example, when a drone is not flying directly towards the radar, the radial velocity will be much lower and the drone can be mistakenly classified as a bird, leading to a miss.

The covered literature shows that not much research has looked at detection algorithms with regards to drone detection. Possibly, the literature may be classified for military purposes. The next chapter will go into detail on explaining the underlying principles behind FMCW/CW radars.

3 Radar Theory

The first part of this chapter will go into detail explaining the underlying principles behind FMCW and CW radars. The second part of this chapter will focus on the construction of an S-Band FMCW/CW radar.

3.1 Antenna theory

An antenna converts electrical signals into radio signals, in transmission mode and radio signals back to electrical signals in receiving mode. The received signal may contain important information about the range and speed of an object of interest. In this project, a quarter-wave monopole antenna will be used. This is one of the most common monopole antennas. The monopole antenna is simply a straight copper wire connected to a coaxial cable which is used for transmitting electrical signals.

Instead of radiating energy in all directions, the monopole antenna is placed inside a cylindrical waveguide to concentrate the energy in a specific direction, towards an object of interest. Without a waveguide, the power of the electrical signal would decrease according to the inverse square law, and the return signal would be too small to measure and difficult to differentiate from noise.

From waveguide theory, when a transverse electromagnetic wave is launched inside a circular waveguide, the TEM wave will not propagate down the structure as this would break two of the boundary conditions that arise from Maxwell's equations which states that:

- A tangential electric field must vanish or terminate at the boundary of a perfect conductor
- Any magnetic field that is normal to a perfectly conducting boundary must also terminate at the boundary

The above is valid for a transverse electromagnetic wave propagating in one direction. Since a monopole antenna radiates radio waves in all directions, two waves propagating in specific directions will superimpose to meet the boundary conditions.

For effective transmission and reception, the distance between the antenna and the back wall of the waveguide should be $\frac{1}{4}$ the waveguide wavelength (λ_g). The monopole wire should be $\frac{1}{4}$ the wavelength of the centre frequency (λ_o) in length.

$$\lambda_g = \frac{\lambda_o}{\sqrt{1 - (\frac{\lambda_o}{\lambda_c})^2}} \quad (3.1)$$

Where $\lambda_c = 1.705 D$ for a cylindrical waveguide operating in TE11 mode and $\lambda_o = c/f_o$

D is the diameter of the cylinder and f_o is the centre frequency of operation of the radar.

The cut-off frequency is the lowest frequency allowed to propagate through a waveguide. For a cylindrical waveguide, the cutoff frequency is given by:

$$f_c = c/\lambda_c \quad (3.2)$$

The S11 parameters of an antenna are used as a measure of efficiency. The S11 parameters are ratios of the reflected power to the transmitted power at different frequencies and will be used in this project to set the design goals for the antenna.

3.2 CW and FMCW Theory

Once the high-frequency wave radiated from the antenna hits a moving object, the reflected wave will be shifted in frequency due to the doppler-effect. The size of the frequency shift is proportional to the speed of the moving object. The Doppler effect is essential to understand the operation of CW and FMCW radars.

Continuous Wave (CW) Radar

A continuous-wave radar transmits signals continuously, at a constant frequency. There is no way of telling the range of an object using this radar. Consequently, CW radars are used for measuring only the speed of the target.

The circuit realization of a CW radar is shown below:

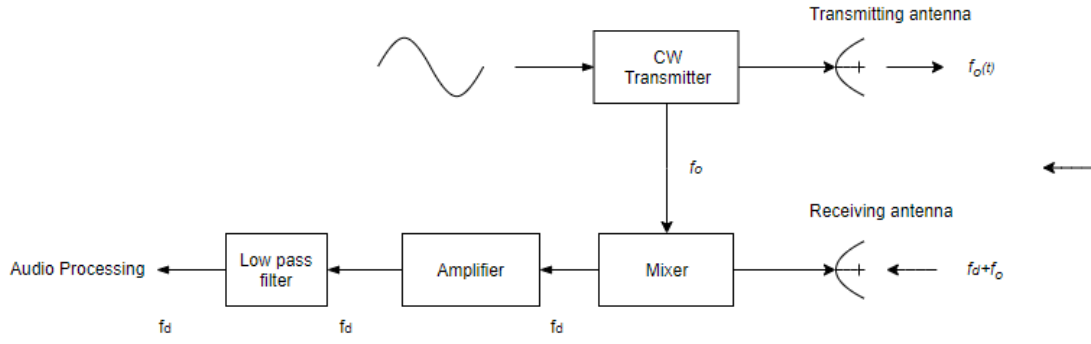


Figure 8: Circuit realisation of a CW radar

In Fig. 8, the CW transmitter produces a signal that is at a frequency of f_o . When the signal hits the moving target in the direction of the radar, the return signal will be doppler shifted to a frequency of $f_o + f_d$. The mixer will modulate the signal to baseband and the output signal will be amplified before passing through the low pass filter. The output of the low pass filter used for audio processing.

In a CW radar, the rate of change of phase of the return signal is used to determine the speed of the moving target. The phase is given by:

$$\phi(t) = 4\pi \frac{r(t)}{\lambda} \quad (3.3)$$

Where $r(t)$ is a measure of the distance travelled by the wave and λ is the wavelength of the transmitted signal.

By calculating the rate of change of the phase of the echo signal, the following is established:

$$\frac{d\phi(t)}{dt} = \omega_d = 2\pi f_d = \frac{4\pi}{\lambda} * v_r \quad (3.4)$$

Rearranging the equation above gives the radial velocity as:

$$v_r = \frac{f_d c}{2f} \quad (3.5)$$

This is the relationship between the doppler frequency and the radial velocity of the target. The next section will look at FMCW radars which are slightly more advanced.

Frequency Modulated Continuous Wave (FMCW)

A radar in FMCW mode will transmit a bandlimited chirp signal. A chirp is a signal with frequency increases and/or decrease. Therefore, the received signal will also be a delayed chirp. The difference in frequency between the transmitted and received signal at a point in time is the beat frequency. The beat frequency contains the information of the range and speed of the moving object and can be found by using a frequency counter. Alternatively, one can run an FFT on the received signal to identify the beat frequency. The circuit realization of a radar in FMCW mode is shown below

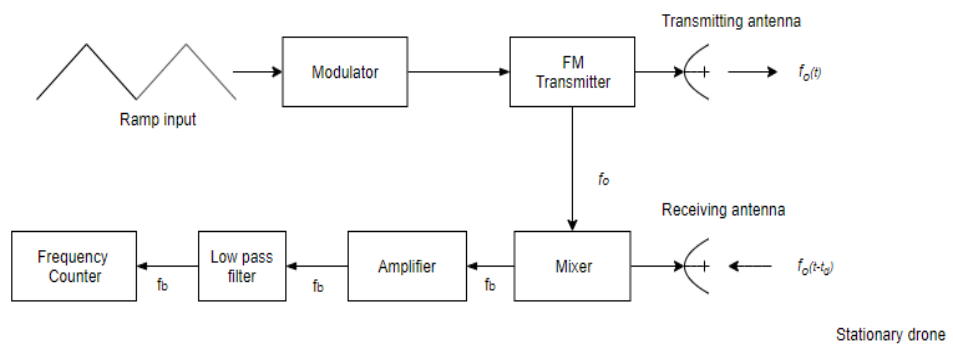


Figure 9: Circuit realisation of FMCW radar

For a stationary target, the transmitted and return signals are shown in Fig. 10 and the beat frequency is calculated.

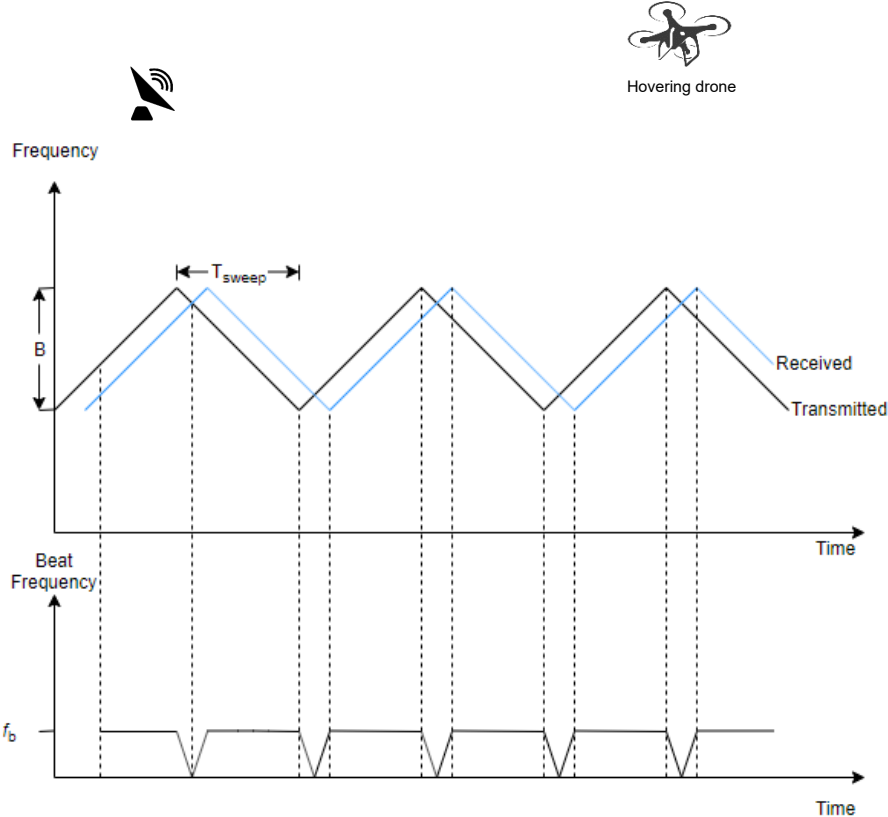


Figure 10: Stationary drone frequency readings

After determining f_b , the range is then determined from the following equation:

$$R = \frac{cT_{\text{sweep}}f_b}{2B} \quad (3.6)$$

where T_{sweep} is the sweep time, f_b is the beat note and B is the bandwidth.

For a moving target, the received signal will be time and frequency shifted. As a result, there are two different beat notes in the received signal as shown in Fig. 11. The beat frequency will be half-way between the two beat notes.

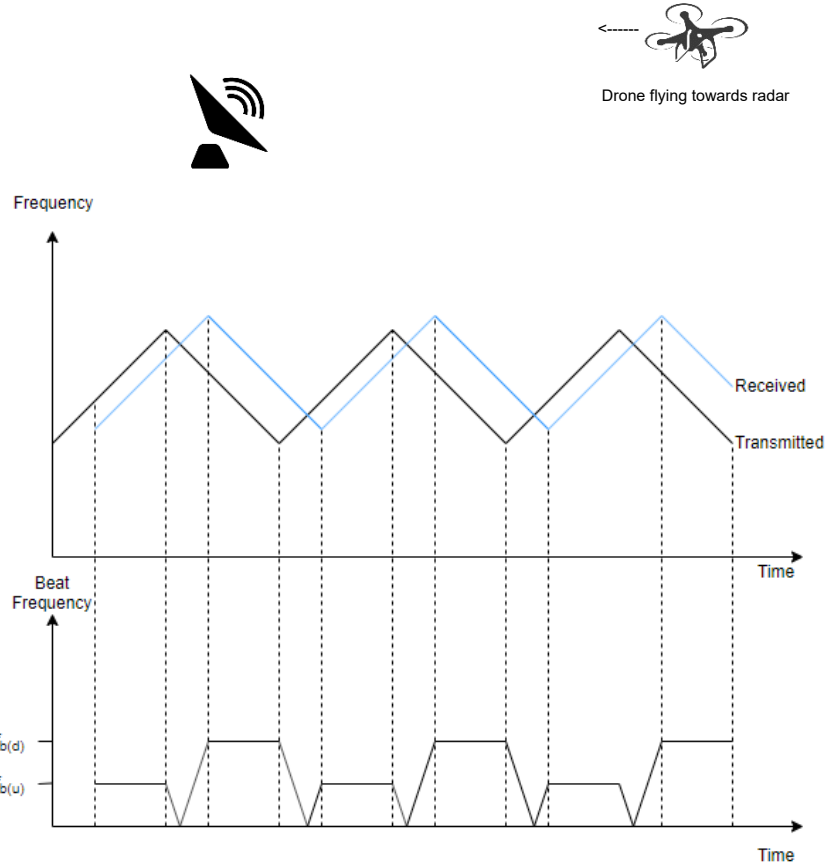


Figure 11: Moving drone frequency readings

The range is then calculated from the equation below.

$$R = \frac{c T_{sweep} (f_{b(u)} + f_{b(d)})}{4B} \quad 3.7$$

where T_{sweep} is the sweep time, $f_{b(u)}$ is the lower beat note, $f_{b(d)}$ is the higher beat note and B is the bandwidth.

The range resolution of the radar is:

$$\Delta R = \frac{c}{2B} \quad 3.8$$

The maximum unambiguous range is:

$$R_{un} = \frac{cT_{sweep}}{2} \quad 3.9$$

Having discussed the principles behind FMCW and CW radars, the following section will focus on constructing an FMCW/CW radar.

3.3 Radar Construction

The radar for this project is expected to operate in the range 2.4-2.5 GHz (S-Band), which is a high frequency. High-frequency signals allow for the use of smaller sized antennas, which are much easier to build compared to bigger antennas.

The radar construction process will follow the steps outlined in the MIT IAP 2011 documentation [3]. Changes will be made where alternative approaches can be used without affecting the design goals. It is important to note that the MIT radar was chosen because it is cheaper to construct hence more affordable for the limited budget.

The following subsections will be covered

1. Antenna design and testing
2. High-frequency circuit design
3. Low-frequency circuit design and testing
4. PCB implementation of low-frequency circuit
5. Assembling and testing the radar

Antennas

3.3.1.1 Antenna Design

Building the antenna requires the following materials

1. Two Milo cans
2. Short copper wire
3. Microwave connector

The antenna building procedure followed the steps stipulated on the antenna website [9], which are similar to those outlined in the MIT documentation. However, different sizes of cans were used together with different connectors. Thankfully the body of the antenna was prepared by Dr Schonken's postgraduate students. The antenna wire length would be adjusted to meet the design specifications.

3.3.1.2 Specifications

The reflection coefficient at the input port (S11 parameter) should be less than -10dB, between 2.4 and 2.5 GHz. This means less than 10% of the transmitted power is reflected while the rest is transmitted.

3.3.1.3 Design

There are three crucial parameters to take note of when designing the antenna:

- the size of the milo cans,
- the distance of the monopole wire from the back wall and
- the length of the monopole wire.

The Milo cans used in this are different in size from the ones used in the MIT documentation. This is allowed since the length and diameter of a can only affect the half-power beamwidth and the shape of the beamwidth. This does not prevent meeting the design specifications. The dimensions of the milo cans used are as follows:

- Length (L) = 15.4 cm
- Aperture Diameter (D) = 10 cm

The following section will look at the calculation done to determine the required length of the monopole wire, together with the distance from the back wall.

3.3.1.4 Calculations

To meet the design goals, the length of the monopole pin should be $\lambda_o/4$, while the distance from the back wall should be to $\lambda_g/4$ for an operating frequency of 2.45 GHz.

The wavelength in free space is given by:

$$\lambda_0 = \frac{c}{f} = \frac{3 * 10^8}{2.45 * 10^9} = 0.122 \text{ m}$$

The cut-off wavelength is given by:

$$\lambda_c = 1.705D = 0.1705 \text{ m}$$

The cut-off frequency is, therefore:

$$f_c = \frac{c}{\lambda_c} = 1.760 \text{ GHz}$$

Waveguide wavelength:

$$\lambda_g = \frac{\lambda_0}{\sqrt{1 - (\frac{\lambda_0}{\lambda_c})^2}} = 0.175 \text{ m}$$

The calculated cut-off frequency was 1.76GHz, which is below the operating frequency of 2.45 GHz. Therefore, the milo cans could be used as a waveguide.

The monopole pin length should be:

$$\frac{\lambda_0}{4} = 0.031 \text{ m}$$

Monopole spacing from the wall should be:

$$\frac{\lambda_g}{4} = 0.044 \text{ m}$$

From these calculations, the length of the monopole should be **31 mm** and the spacing from the back wall **44 mm** to meet the design goals. The diagram below shows a Solid Works implementation of the antenna.

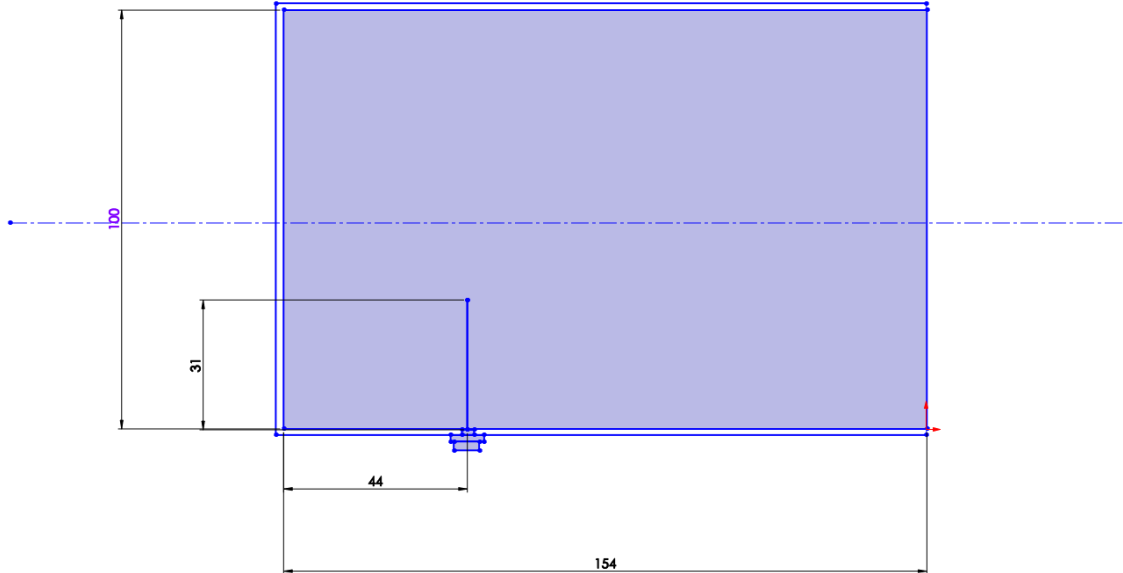


Figure 12: Solid works diagram of the antenna (mm)

3.3.1.5 Connector

A Flange Mount SMA Connector was used since the N-Female Chassis Mount Connector used on the website was not available. The SMA connector will act as a perfect substitute of the Chassis Mount connector for the transmission of electrical signals. The diagram below shows the connector used.

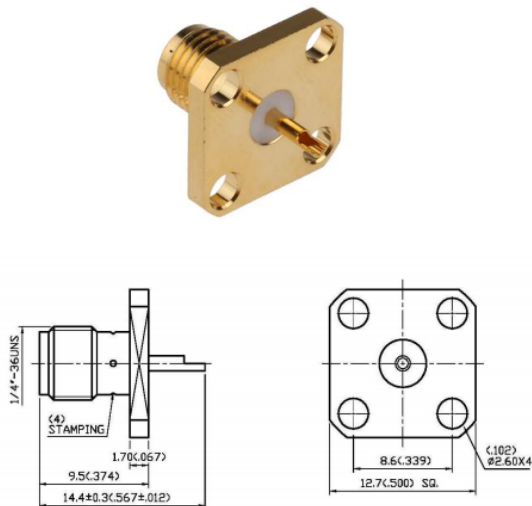


Figure 13: Flange Mount SMA Connector. Adapted from [10]

3.3.1.6 Monopole pin

The monopole pin is a short piece of copper wire that was trimmed to the required length. The copper wire was soldered to the SMA connector to ensure a good connection. The following pictures show the prepared antenna.



Figure 14: Interior of the antenna



Figure 15: Exterior of the antenna

3.3.1.7 Testing and Tuning Antennas

To test the S11 parameters, a Spectrum and Vector Network Analyser from the UCT Microwaves laboratory was used. Both antennas were tested. Initially, the S11 parameters between 2.4 and 2.5 GHz were found to be higher than -10 dB as shown in Fig. 17. The copper wire was then trimmed sparingly using a cutter while checking the effect of the changes on the screen. This was done until the S11 parameters were satisfactory for both antennas. Final results are shown in Fig. 18.

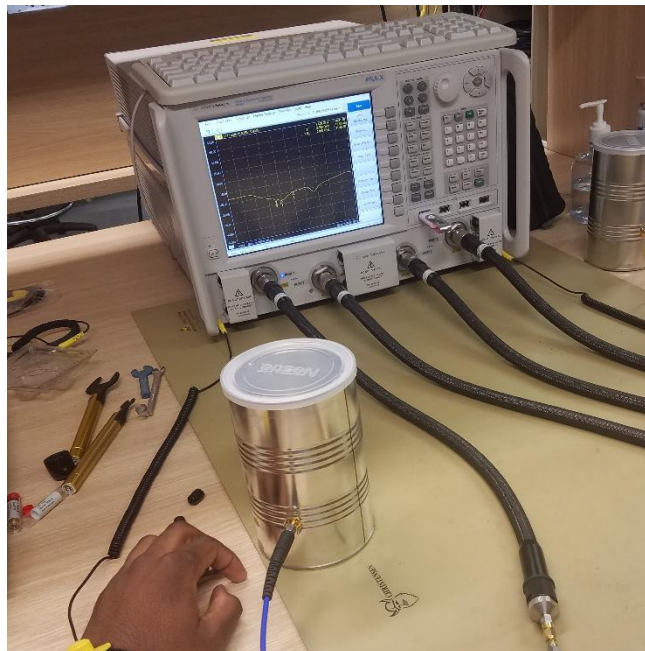


Figure 16: Antenna testing equipment

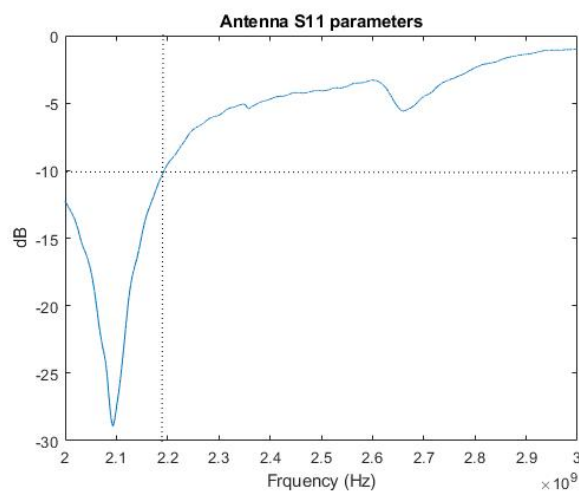


Figure 17: Antenna S11 before tuning

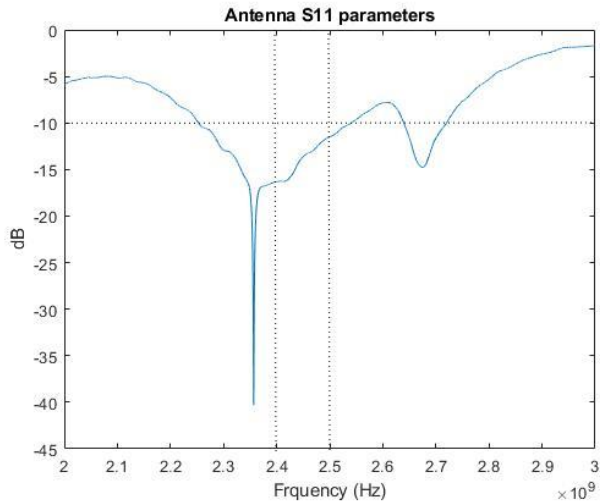


Figure 18: Antenna S11 after tuning

The trimming process resulted in monopoles that were roughly 27 mm long, different from the simulated 31 mm. This is because equations from simulation models are for ideal conditions and the assumptions made will always have a margin of error.

High-frequency circuit

Ordinary capacitors and resistors do not behave as expected at high frequencies. Therefore, to build a high-frequency circuit, specialised components that can handle high frequencies are required. These components were bought form Minicircuits.

The high-frequency components are as follows:

- Voltage Controlled Oscillator (VCO) – Produces a frequency modulated signal having a variable frequency. The input to the VCO is a triangular wave which excites the VCO
- Attenuator – Improves the impedance matching between the VCO and Amplifier 1
- Amplifier 1 – Amplifies the signal to improve power for transmission
- Splitter – Creates a copy of the transmitted signal to be sent to the mixer
- Amplifier 2 – Amplifies the received signal that will be at very low power to increase its power
- Mixer – multiplies the transmitted signal and the received signal to get the baseband signal

The Minicircuit components are powered by 5 V. The two figures below show how the components are connected in drawing and in implementation.

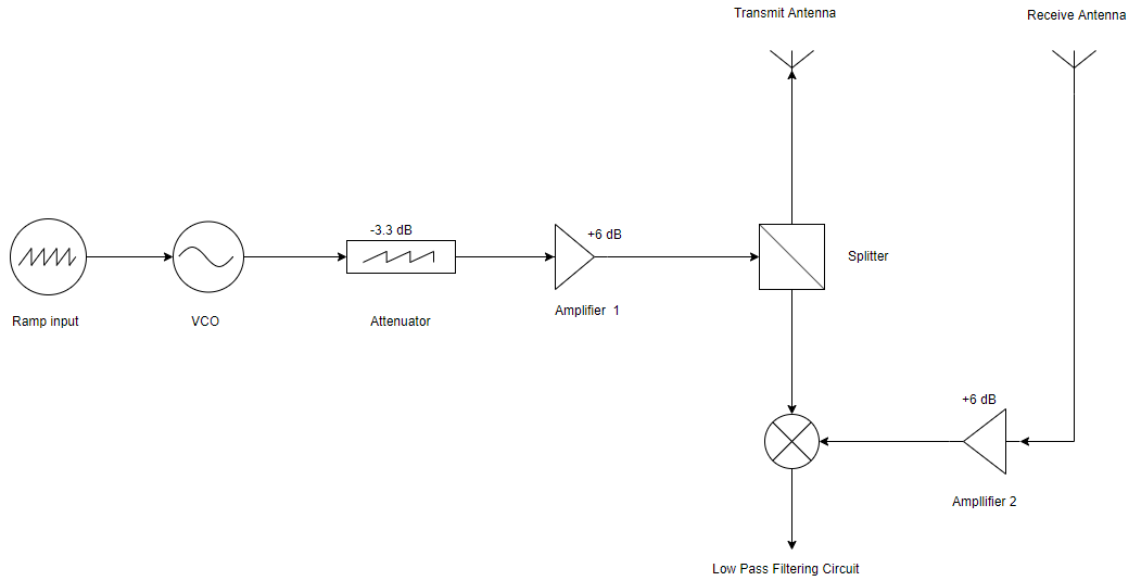


Figure 19: High-frequency circuit

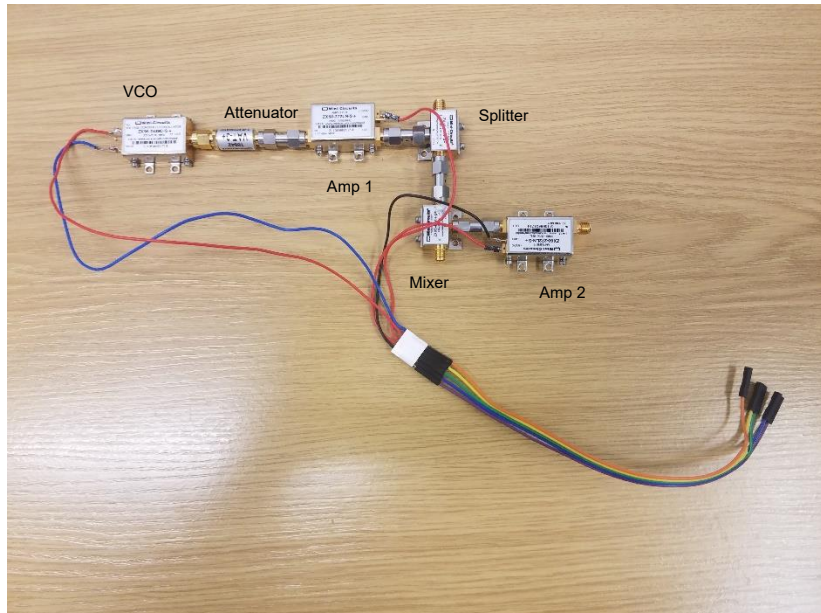


Figure 20: High-frequency circuit implemented

A table of components together with the part number of each component are shown below.

Table 2: High-frequency parts and their part number

Part	Part Number
VCO	ZX65-2536C+
Attenuator	VAT-3+
Amplifier 1	ZX60-272LN+
Splitter	ZX-10-2-42+
Mixer	ZX05-43MH+
Amplifier 2	ZX60-272LN+

Low-frequency circuit

The low-frequency circuit consists of three sections:

1. Voltage regulator circuit – For powering the circuit
 2. Active Low Pass Filter – For filtering out high-frequency signals and amplifying the baseband signal.
 3. Ramp Generator – Used to produce the triangular wave signal that is used as a modulating signal for the VCO.

The low-frequency circuit should

- Perform low pass filtering on the base-band receive signal with a cut-off frequency of 15 kHz
 - Generate a square wave of 50 Hz frequency used as a clock signal and a 50Hz triangular wave used for modulation
 - Provide 12V and 5V regulated power

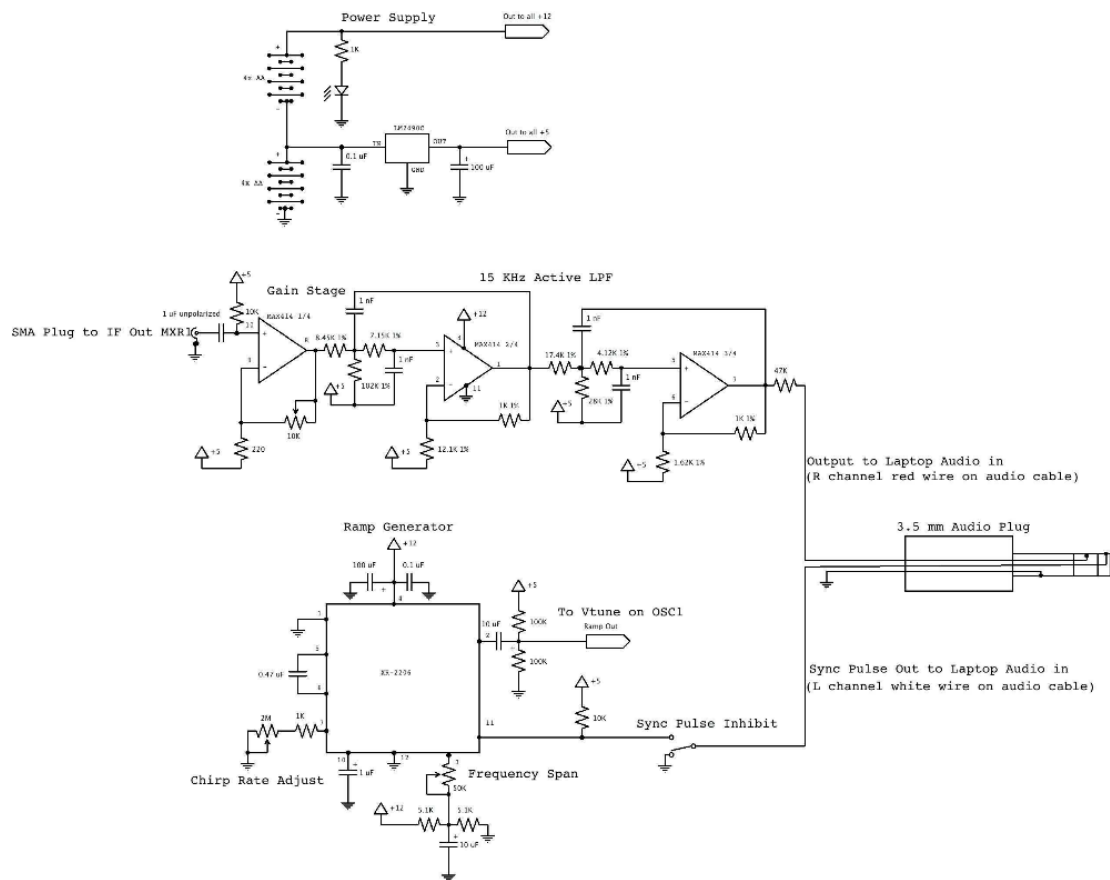


Figure 21: Low-frequency circuit. Adapted from [3]

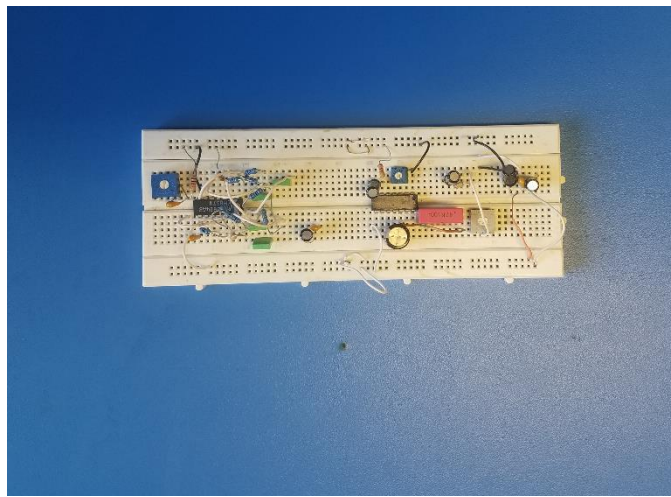


Figure 22: Breadboard circuit

3.3.1.8 Voltage regulator circuit

Building

The LM2490 5V regulator suggested in the MIT documentation was not available and instead, an LM7805 5V voltage regulator was used to power the circuit. The voltage regulator is connected to an LED that is used to indicate if the system has been powered. In implementing the circuit, a heat sink was attached to the voltage regulator to ensure that energy is dissipated easily, thereby preventing overheating.

Instead of using two packs of 4AA batteries, one for 6V and then 12V in the MIT plans, a 12V, 1.2Ah lead-acid battery was used which was available in the UCT Whitelab.

Testing

The circuit was tested in the Whitelab, and the following data was collected.

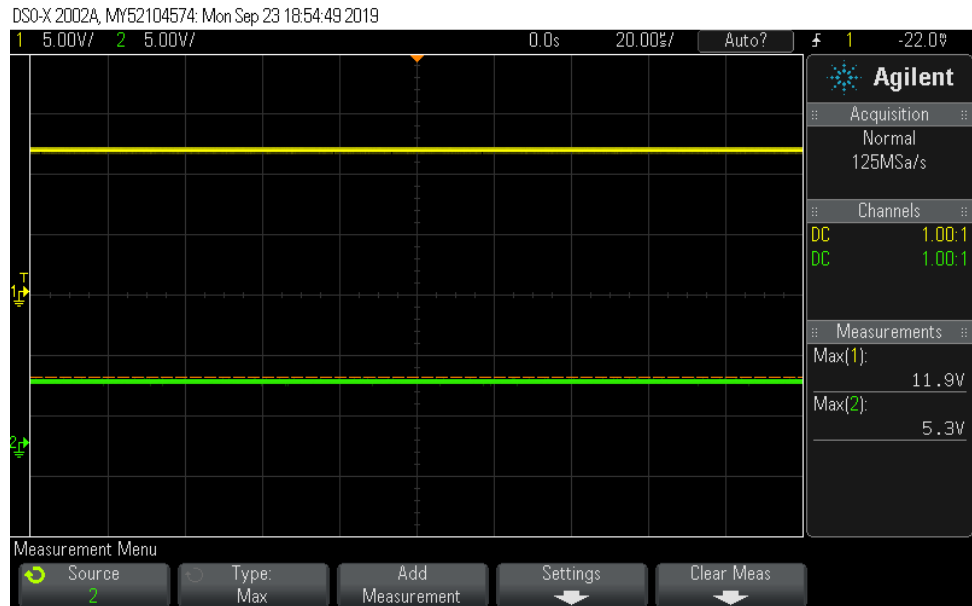


Figure 23: Voltage regulator results

The voltage regulator circuit was working as expected as it produced 11.9 V and 5.3 V which are close to 12V and 5V. The difference is negligible and will be ignored

Active low pass filter circuit

Building

The active low pass filter circuit consists of an initial variable gain section (amplifier) and two Sallen-Key configured circuits that are responsible for filtering out high-frequency signals. As a result high-frequency noise signals are filtered out before sampling by an ASUS Xonar U3 USB sound card.

The LM837N chip was used for implementing this circuit instead of the MAX414 quad op-amp proposed in the MIT design. This was done because the MAX414 is expensive and could not be sourced. The two op-amps have almost similar gain bandwidths hence could be interchanged with the LM837N having a bandwidth of 25 MHz and MAX414 with a gain bandwidth of 28 MHz.

Resistor selection – E96, 1% resistors were available and were used to implement the circuit.

Testing and tuning

All testing was done on the breadboard before implementing the whole circuit on the PCB. A DSO-X2002A oscilloscope was used to display the results.

Gain circuit Testing

Initially, the gain circuit was tested using a sinusoidal signal of amplitude 1V, and frequency 15 kHz coming from a Whitelab signal generator. The potentiometer was adjusted until the output of the circuit was at a maximum, just before clipping. The output of the gain circuit was a sinusoid of amplitude 5.8 V as shown in Fig.24. This is a gain of about 5.74.

DSO-X 2002A, MY52104574: Mon Sep 23 18:53:40 2019

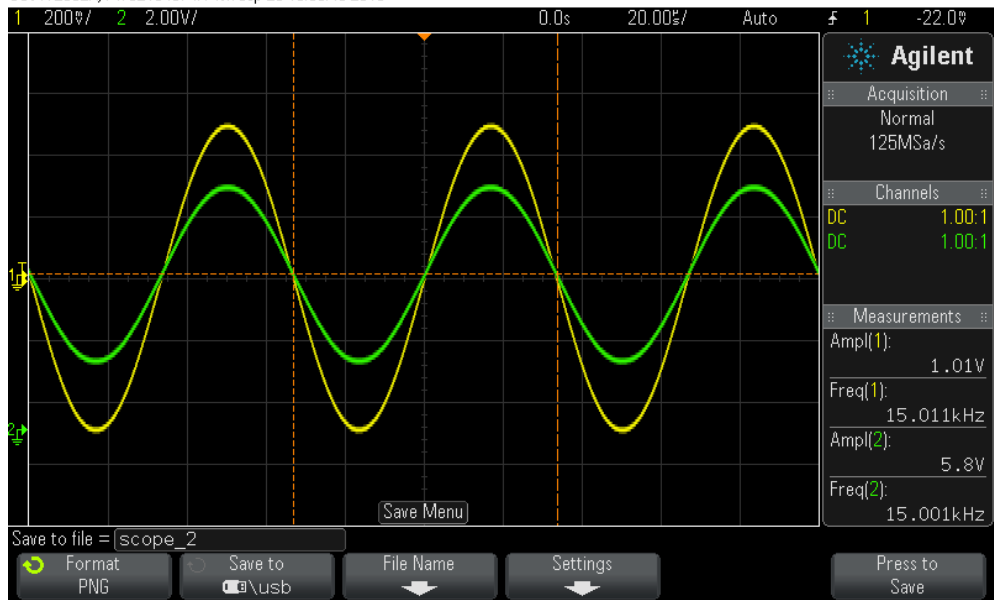


Figure 24: Gain circuit results

Filtering Circuit Testing

To test the filtering properties of the filtering circuit, a 5.65 V amplitude was measured at the input of the Sallen-Key configured circuit, with a 1 V amplitude, 15 kHz sinusoidal signal at the input of the gain circuit. The output was recorded and had an amplitude of 4 V as shown in Fig. 25.

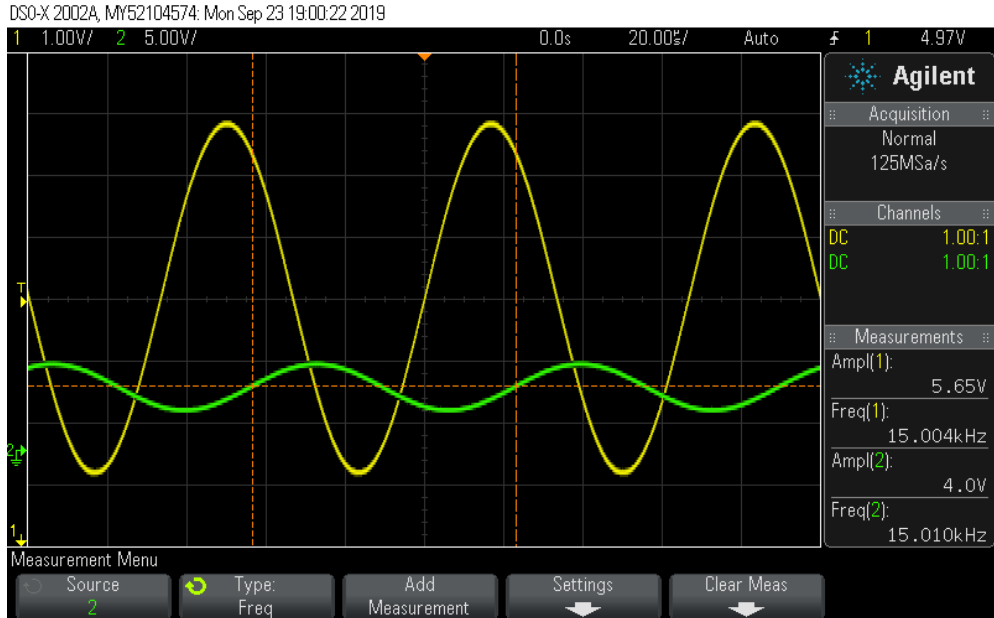


Figure 25: Filtering circuit results

The gain was calculated as

$$G_{dB} = 20 \log \left(\frac{4}{5.65} \right) = -3 \text{ dB}$$

The gain was found to be -3 dB at the cut-off frequency hence the circuit was working as expected. The output of the filtering circuit is connected to the right channel which is the red wire on the audio cable.

Signal generator circuit

Building

As in the MIT documentation, the XR-2206 function generating chip was used for generating both the triangle wave, used for modulation and the square wave, used for synchronization. The signal generator circuit has two outputs. The ramp output goes to the V-tune input of the VCO and the square signal output goes to the Left channel(blue wire of audio cable).

The circuit has two potentiometers that are used for varying the pulse length of the chirp signals ($2M\Omega$ potentiometer) and adjusting the peak to peak value of the triangular modulating wave($50k\Omega$).

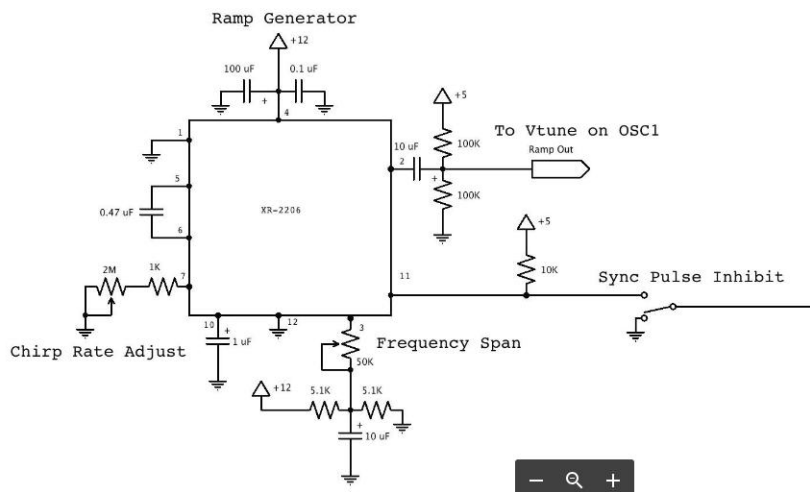


Figure 26: Signal generator circuit. Adapted from [3]

Testing the ramp and square wave

The $50 k\Omega$ potentiometer was adjusted to ensure that the ramp amplitude could be varied between 0 and 5 V, centred at 2.5. This was confirmed. The potentiometer was then set using the datasheet of the VCO.

V TUNE	TUNE SENS (MHz/V)	FREQUENCY (MHz)		
		-55°C	+25°C	+85°C
0.00	81.90	2267.6	2257.4	2249.2
0.50	74.61	2306.7	2297.3	2289.5
0.75	73.96	2325.2	2315.9	2308.2
1.00	73.76	2344.0	2334.4	2326.4
1.25	73.75	2362.7	2352.9	2344.6
1.50	74.01	2381.6	2371.3	2362.6
1.75	74.71	2400.7	2389.8	2380.6
2.00	74.15	2419.7	2408.5	2398.9
2.25	73.21	2438.5	2427.0	2417.2
2.50	71.91	2456.9	2445.3	2435.4
2.75	70.82	2475.0	2463.3	2453.3
3.00	68.45	2492.6	2481.0	2471.1
3.25	65.44	2509.4	2498.1	2488.3
3.50	61.36	2525.2	2514.5	2504.9
3.75	57.60	2540.3	2529.8	2520.7
4.00	53.56	2554.4	2544.2	2535.4
4.25	50.01	2567.6	2557.6	2549.0
4.50	45.62	2579.9	2570.1	2561.7
4.75	41.10	2591.0	2581.5	2573.3
5.00	36.26	2601.0	2591.8	2583.8

Figure 27: Excerpt of Minicircuits VCO. Adapted from [11]

From the excerpt above, a modulating triangular signal that is centered at 2.5 V with a peak to peak voltage of 1.5 V would allow the frequency shift within the operating region. As a result, the bandwidth is simply $(2498.1 - 2389.8)$ MHz which is approximately 108.3. The bandwidth was rounded up to 109 MHz.

The 50 KΩ potentiometer was then adjusted until it gave a peak-peak output of 1.5 V centred at 2.5 V.

To set the frequency of the square wave and the triangular wave to 50 Hz, the 2MΩ potentiometer was the adjusted. After the adjustment, the two outputs were then compared to see if both modulating and square wave signals were in sync.

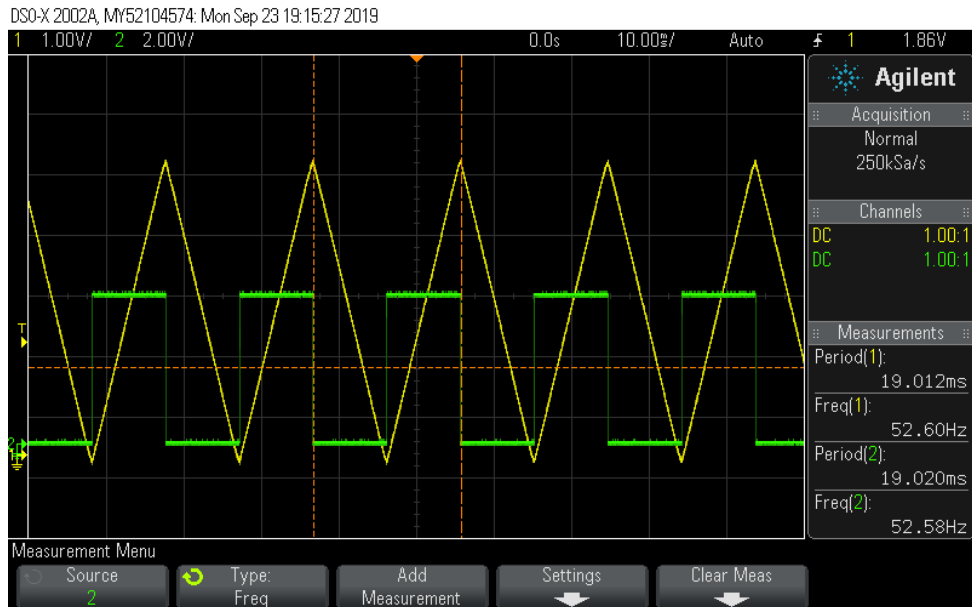


Figure 28: Signal generator circuit results

As shown in Fig. 28, the two outputs were in sync, hence the circuit was working as expected. As soon as all the components were confirmed to be working, the next step was designing the PCB and populating it with components.

PCB Design

Given that Adrian's breadboard circuit was working and passed all the circuit test, it was decided that the circuit be implemented on a PCB to save time. The PCB circuit was expected to do the following:

- Linear filtering with a cut-off frequency of 15 kHz
- Allow powering with a 12 V lead-acid battery, 1.2Ah
- Switch between FMCW and CW mode
- Connect to the transmitting antenna through an SMA coaxial connector
- Allow easy debugging with the use of test points

The PCB schematic is shown below:

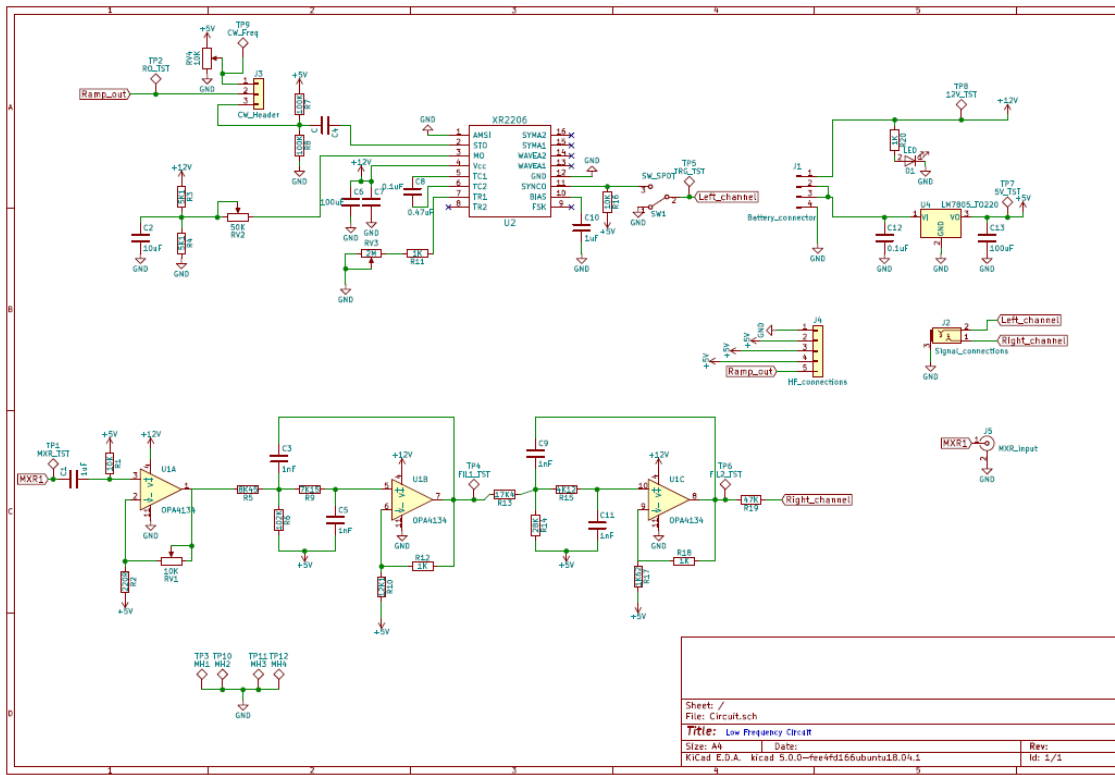


Figure 29: PCB schematic

The only change made to the PCB was change in header pins. It was decided that 2.54 mm headers be put so that it is easier to pull out and put jumpers on the PCB when switching between CW and FMCW mode.

The PCB board is shown below.

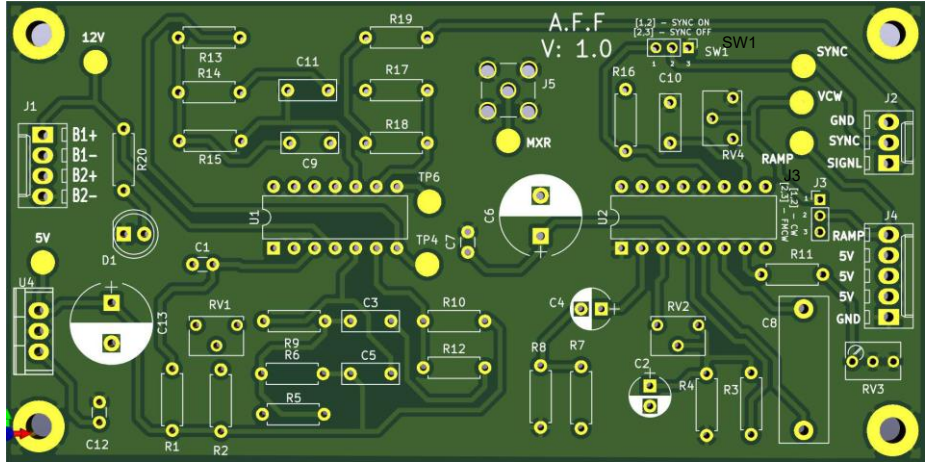


Figure 30: PCB before being populated

It is important to note that in FMCW mode, the jumpers will connect headers 1 and 2 to turn the sync on (at SW1 on the board) and connect headers 2 and 3 (at J3). In CW mode, the jumpers connect headers 2 and 3 (at SW1) to turn the sync off and connect headers 1 and 2 at J3.

After receiving the PCB from TRAX, the PCB was populated with components used for the breadboard circuit. The picture is shown below.

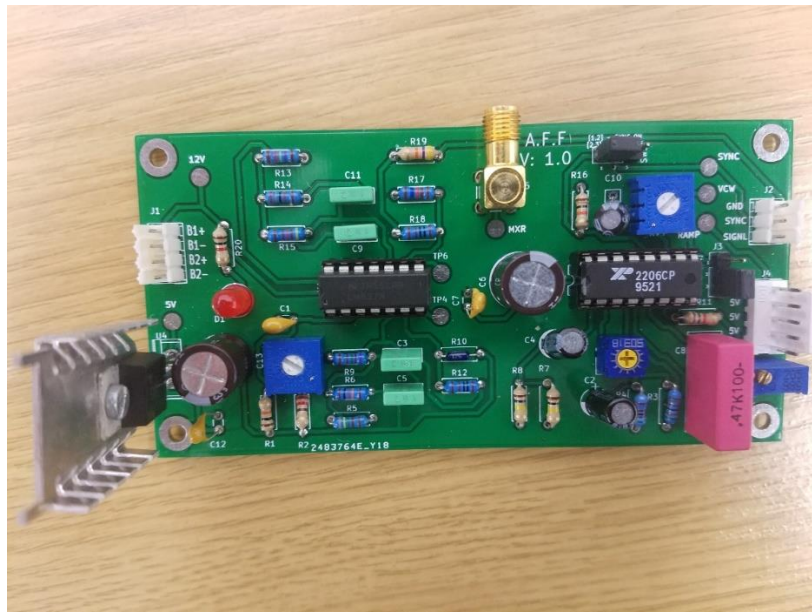


Figure 31: PCB after population by components

The signal generator and low pass filtering circuit were tested again as in the previous sections and the results were similar to those found in the breadboard circuit tests. The

output of the triangular modulating signal was in sync with the clock signal and was centred at 2.5 V with a peak to peak voltage of 1.5 V, and a frequency of 50 Hz.

Base and Assembly

The base was constructed using a piece of wood with dimensions $45 \times 30 \times 1.5 \text{ cm}^3$. L-brackets were purchased from Builder Express and were used to mount the antennas on the base. The antennas were then connected to the RF circuit. The pictures below show the radar after assembly.

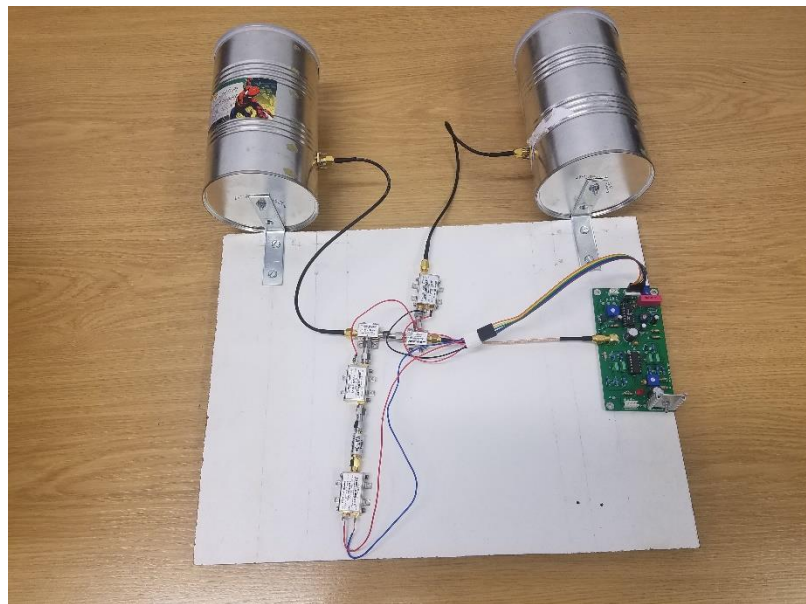


Figure 32: Radar before enclosing



Figure 33: Radar after enclosing

Testing the radar

To check if the radar was working as expected, four simple tests were carried out. In the FMCW mode the following tests were done:

1. A person walking away from the radar to the wall of the Whitelab (about 8.5 m away from the radar)
2. A person walking away towards the wall, and then back. The results are as shown below.

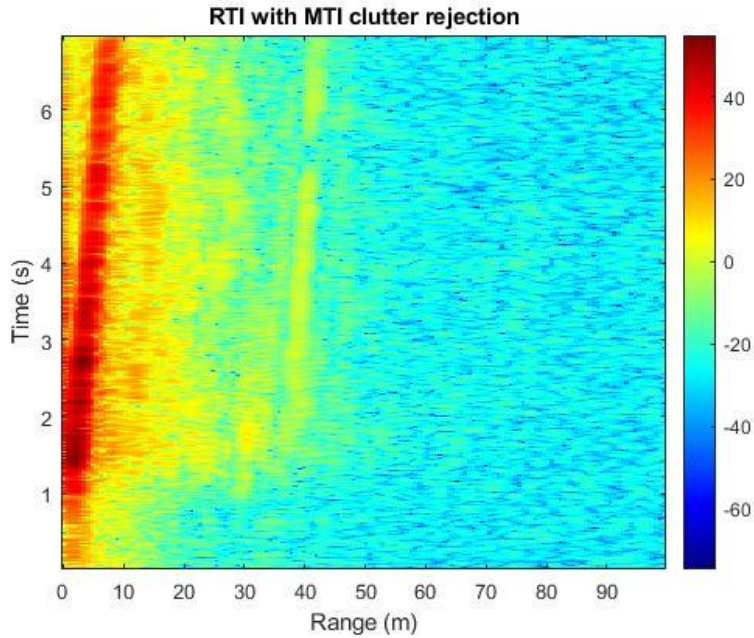


Figure 34: Person walking away from the radar (range detection)

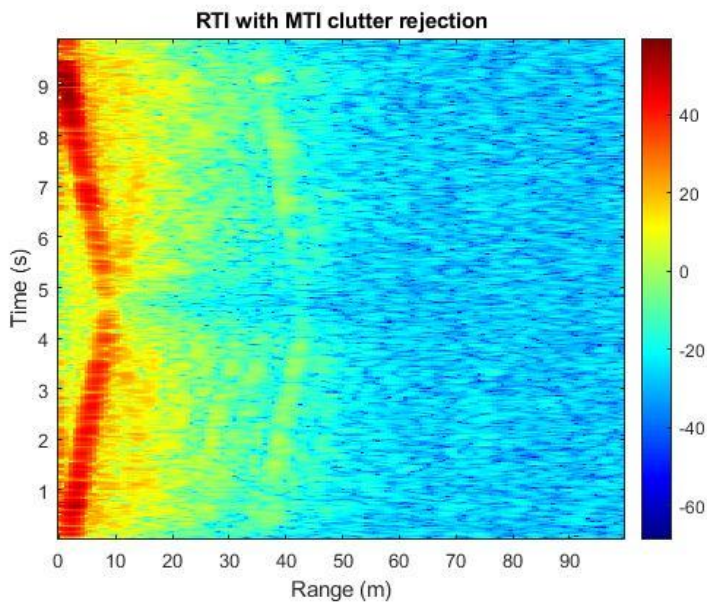


Figure 35: Person walking away and then towards the radar (range detection)

In CW mode, similar tests were carried out with a person walking away from the radar and then walking away and towards. The results are shown below.

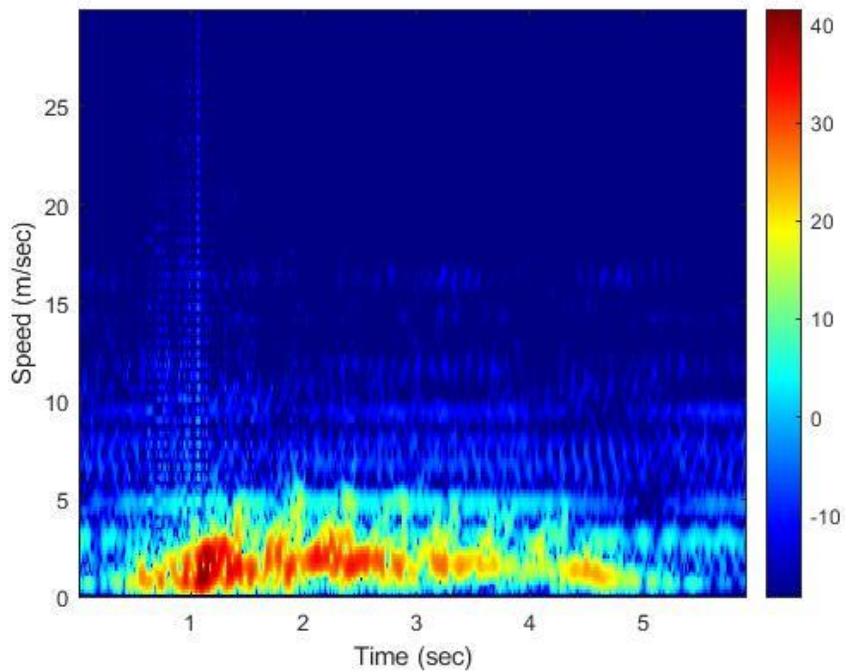


Figure 36: Person walking away from the radar (speed detection)

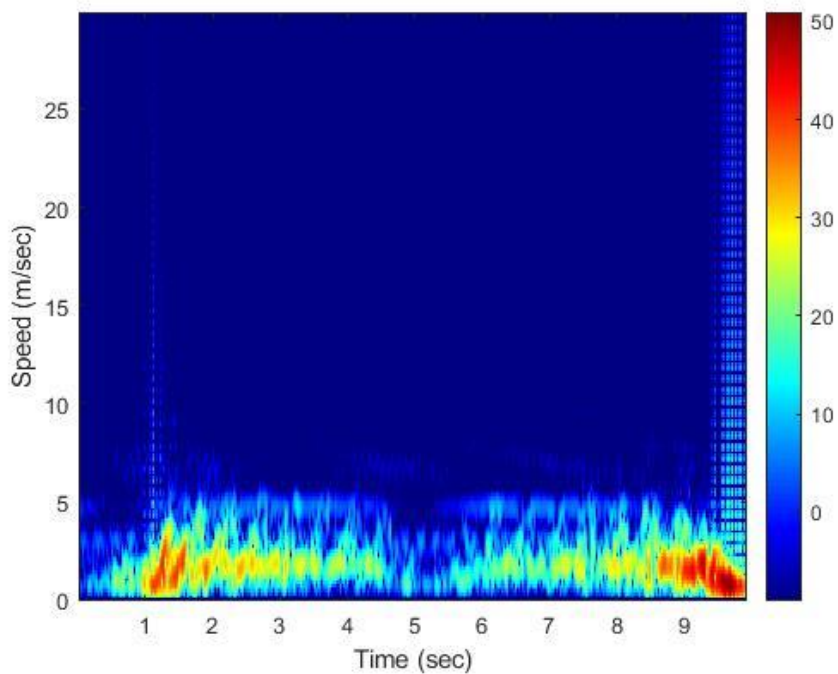


Figure 37: Person walking away and then towards the radar (speed detection)

The results confirmed that the radar was working as expected.

4 Detection Theory

In FMCW mode, the received data is processed into range lines. The range lines are stored as a matrix of complex values that indicate magnitude and phase of the received signal in each cell. This Chapter will focus on manipulating the complex data to get to a detection decision.

4.1 Linear and Square Law Rectifiers

Linear law rectifier

Given the I and Q values for each range cell, linear rectifiers calculate the absolute value of the complex reading. That is,

$$y = \sqrt{I^2 + Q^2} \quad (4.1)$$

Linear rectification is computationally expensive. The output, y can be interpreted as a voltage value.

Square law rectifier

Square law rectifiers only calculate the square of the absolute value of the complex reading. Thus,

$$y = I^2 + Q^2 \quad (4.2)$$

There are fewer computations involved with a square-law detector and this is one of the reasons square law rectifiers are more common than linear rectifiers. Furthermore, for Rayleigh distributed interference, which is a very common type of interference, the maximum likelihood estimator of the interference power takes the form of a square-law detector. This makes detection calculations simpler. The output of a square law rectifier can be interpreted as a measure of the power value.

4.2 Threshold Detection of Radar Targets

Once the output value of each range cell has been passed through the rectifiers, the next step involves making a detection decision. Detection refers to the processing of readings to determine if the received data only contains interference or if it is a combination of

interference and the target returns. In making a detection decision, a measurement is made on each range cell, and the following hypotheses are investigated

1. H_0 , the measurement only contains interference, that is $y = n$
2. H_1 , the measurement contains interference and target returns, that is $y = n + s$

A threshold is set as an estimate of the noise level that is expected in each range cell. The threshold is then compared to the rectifier outputs. If the measurement is greater than the threshold, then a target is declared present. The measurement is classified under H_1 . If the threshold is higher than the measured value, then a target is declared absent, and the measurement is classified under H_0 .

When a measurement contains only noise but, is greater than the threshold, a false detection will be made. False alarms cannot be completely eliminated from a system, however, the goal is to ensure that they are kept at a minimum and constant despite the varying noise levels. The goal of a detector is to ensure that the P_{FA} is low and constant while maintaining a high probability of making the correct decision (probability of detection).

4.3 Detectors

The false alarm rate is defined as the product of the number of detection decisions made and the probability of making a false alarm. A higher threshold reduces the probability of false alarm and also the probability of detection, while a lower threshold increases the probability of false alarm and that of detection.

Neyman-Pearson Detector

Neyman-Pearson (NP) detectors have a fixed threshold and are designed to work in an environment where the interference PDF is known together with its parameters. In calculating the threshold, it is assumed that the adjacent cells used only contain interference from the same distribution and no targets. The Neyman-Pearson detector will maximise P_D for the desired P_{FA} . The threshold is given by

$$T = -\ln(P_{FA})\sigma_i^2 \quad (4.3)$$

Where σ_i^2 is the interference power at the output of the square-law detector. As a rule, the general expression for the threshold of a detector is given by

$$T = \alpha g \quad (4.4)$$

Where α is a function of the desired P_{FA} and is called the constant of interference and g is an estimate of the interference level.

The NP detector will not be used for this project as it requires knowledge of the interference distribution and its actual parameters. In most cases, actual parameters of the interference distribution are not known but are estimated. CFAR algorithms are used to estimate these parameters, which would allow setting the threshold dynamically.

CFAR Detectors

CFAR detectors use adjacent cells to estimate the interference levels for each range cell or cell under test. The adjacent cells used are called reference cells, and the noise parameters are usually found by averaging or sorting the reference cells. A diagram outlining the CFAR processes is shown below:

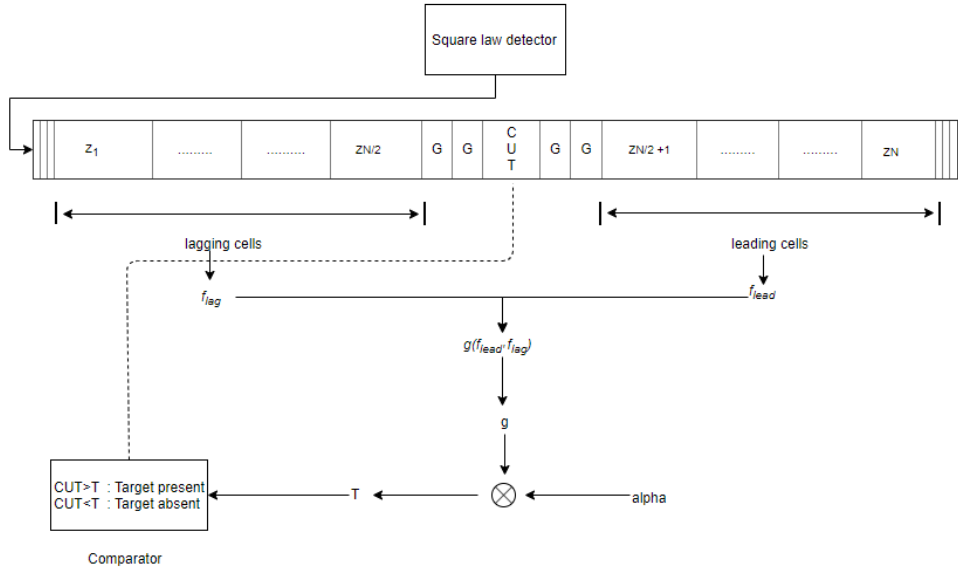


Figure 38: Basic implementation of CFAR algorithms

The Cell-Averaging CFAR (CACFAR)

For each Cell Under Test (CUT), the noise power is estimated using cells to the left and right of the CUT. Guard cells are included to avoid self-masking. CACFAR was designed to give a maximum probability of detection in homogeneous environments and maintain the false alarm rate constant. In homogeneous environments:

1. The interference in the leading and lagging windows and the CUT are independent and identically distributed, meaning the random variable in the interference belong to the same probability density function but would be independent of each other.
2. For every CUT which contain a return from a target, the reference cells do not contain returns from other interfering targets.

The probability of detection of CACFAR is given by:

$$P_{D_{CA}} = \left[1 + \frac{\alpha_{CA}}{N(1 + SNR)} \right]^{-N} \quad (4.5)$$

Where α_{CA} is the CACFAR constant of interference for CACFAR.

The probability of false alarm is found by simply setting SNR equal to zero. This gives

$$P_{FA_{CA}} = \left[1 + \frac{\alpha_{CA}}{N} \right]^{-N} \quad (4.6)$$

For the desired probability of false alarm value, the scaling factor is calculated from equation 4.6 hence:

$$\alpha_{CA} = N \left[P_{FA}^{\frac{-1}{N}} - 1 \right] \quad (4.7)$$

The interference statistic is, therefore:

$$g_{CA} = \frac{1}{N} \sum_{n=1}^N z_n \quad (4.8)$$

The threshold is then a product of the interference statistic and the scaling factor.

$$T_{CA} = \alpha_{CA} g_{CA} \quad (4.9)$$

4.3.1.1 Self-masking

When the target extends beyond one cell, the estimated noise statistic from reference cells will be higher than expected as a result of including target cells in the calculation. This will lead to a miss of a present target. Guard cells allow the reference cells used for calculating the noise statistic to be made up of noise cells only. The noise statistic will then be as low as expected, leading to a lower threshold value and hence a detection. The following diagrams show the effects of including guard cells:

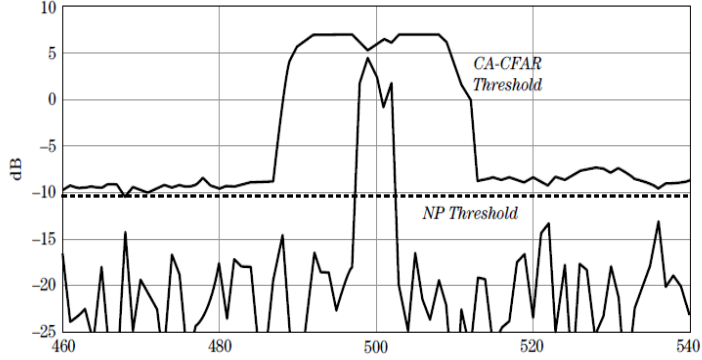


Figure 39: CACFAR without guard cells. Adapted from [12]

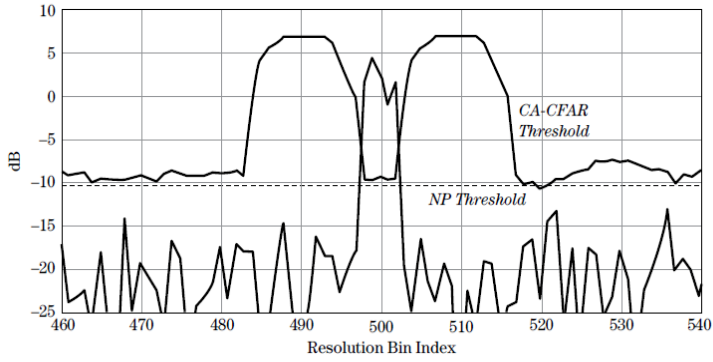


Figure 40: CACFAR after applying guard cells. Adapted from [12]

The number of guard cells is a function of the maximum target extent.

Homogenous conditions are not upheld when there are clutter boundaries and interfering targets. As a result, the adjacent cells used to estimate the noise statistic will not contain noise from the same distribution or may contain returns from other targets. In such cases, CACFAR performance degrades.

4.3.1.2 Clutter boundaries

Abrupt changes of the terrain reflectivity, resulting in abrupt changes of interference are called clutter boundaries(Fig. 41). In CACFAR, this will result in an increase in the P_{FA} as CACFAR will not be able to react quick enough to raise the threshold and will, in turn, give detections at clutter edges. This increases the P_{FA} which is undesirable. Therefore, there is a need for CFARs that can maintain a constant P_{FA} in environments where there are clutter boundaries.

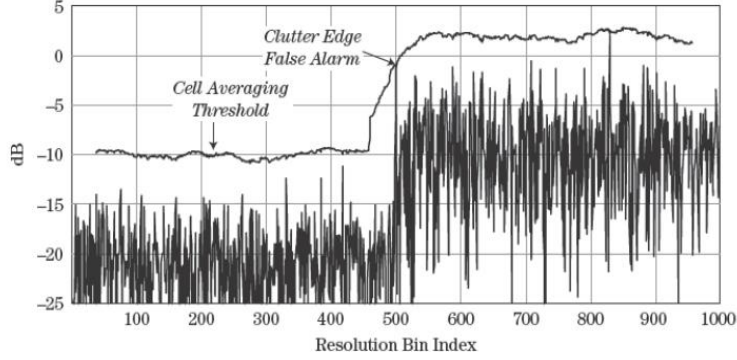


Figure 41: Clutter boundary

GO-CA-CFAR

GO-CA-CFAR is best suited for environments where there are clutter boundaries. The algorithm was designed to reduce clutter edges false alarms [13]. This is achieved by calculating the average interference in lagging and leading cells separately. The CFAR compares between the sum of cells in the lagging and leading windows and the selects the greater of the two to estimate noise statistics. As a result, the threshold will always be higher than that of CACFAR at clutter boundaries. The noise statistic is calculated using the following equation:

$$g_{GO} = \max \left[\sum_{i=1}^{N/2} z_i, \sum_{i=\frac{N}{2}+1}^N z_i \right] \quad (4.10)$$

The probability of detection is given by:

$$P_{D_{GO}} = 2 \left\{ \left[1 + \frac{\alpha_{GO}}{1 + SNR} \right]^{\frac{-N}{2}} - \left[2 + \frac{\alpha_{GO}}{1 + SNR} \right]^{\frac{-N}{2}} \right. \\ \left. * \sum_{k=0}^{\frac{N}{2}-1} \binom{\frac{N}{2}-1+k}{k} \left[2 + \frac{\alpha_{GO}}{1 + SNR} \right]^{-k} \right\} \quad (4.11)$$

The average P_{FA} is found by setting SNR equal to zero, yielding:

$$P_{FA_{SO}} = 2 \left\{ \left[1 + \alpha_{GO} \right]^{\frac{-N}{2}} - \left[2 + \alpha_{GO} \right]^{\frac{-N}{2}} * \sum_{k=0}^{\frac{N}{2}-1} \binom{\frac{N}{2}-1+k}{k} \left[2 + \alpha_{GO} \right]^{-k} \right\} \quad (4.12)$$

To find α_{GO} , iterative methods can be used. The threshold is then defined by

$$T_{GO} = \alpha_{GO} * g_{GO} \quad (4.13)$$

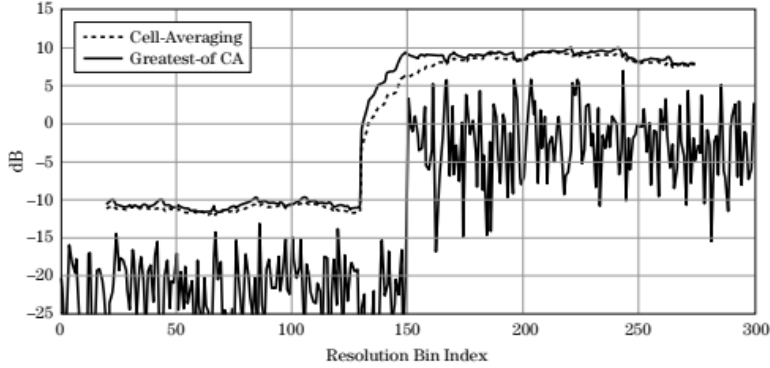


Figure 42: CACFAR and GOCACFAR on clutter edges [12]

However, both GO-CA-CFAR and CACFAR performance is degraded when there is mutual target masking and SOCACFAR was designed to solve the problem of interfering targets.

Smallest-Of CACFAR (SOCACFAR)

SOCACFAR was designed to address the problem of mutual target masking [14]. The algorithm selects the minimum sum between the leading and lagging cells to calculate the interference statistics. This is done to suppress interfering targets in either the leading or lagging windows but not both at the same time. Because the minimum of the two is taken, SOCA does not perform poorly in environments with clutter boundaries.

$$g_{SO} = \min \left[\sum_{i=1}^{N/2} z_i, \sum_{i=\frac{N}{2}+1}^N z_i \right] \quad (4.14)$$

The probability of detection is given by:

$$P_{D_{SO}} = 2 \left[2 + \frac{\alpha_{SO}}{1 + SNR} \right]^{\frac{-N}{2}} * \sum_{k=0}^{\frac{N}{2}-1} \binom{\frac{N}{2} - 1 + k}{k} \left[2 + \frac{\alpha_{SO}}{1 + SNR} \right]^{-k} \quad (4.15)$$

The average P_{FA} is found by setting SNR equal to zero, yielding:

$$P_{FA_{SO}} = 2[2 + \alpha_{SO}]^{\frac{-N}{2}} * \sum_{k=0}^{\frac{N}{2}-1} \binom{\frac{N}{2} - 1 + k}{k} [2 + \alpha_{SO}]^{-k} \quad (4.16)$$

To find α_{SO} , iterative methods can be used. The threshold is then calculated as,

$$T_{SO} = \alpha_{SO} * g_{SO} \quad (4.17)$$

Given that each of the three algorithms, CACFAR, SOCACFAR and GOCACFAR cannot address the problems of interfering targets and clutter boundaries simultaneously, there is a need for robust CFAR's that will tackle this problem.

OS-CFAR

OSCFAR was designed for cases where there are both interfering targets [15] and clutter boundaries or either one of them. For OS-CFAR, the noise statistic is the k th sample of sorted reference cells. OSCFAR is capable of rejecting $N - k$ interfering targets and will suppress clutter edges false alarms provided that $k > N/2$ [16, 17]. Usually, k is chosen to be $3N/4$ thus $N/4$ interfering targets can be suppressed.

The probability of detection is given by:

$$P_{D_{OS}} = \prod_{i=0}^{k-1} \frac{N - i}{N - i + \frac{\alpha_{OS}}{1 + SNR}} \quad (4.18)$$

The probability of false alarm is then:

$$P_{FA_{OS}} = \prod_{i=0}^{k-1} \frac{N - i}{N - i + \alpha_{OS}} = k \binom{N}{k} \frac{(k - 1)! (\alpha_{OS} + N - k)!}{(\alpha_{OS} + N)!} \quad (4.19)$$

The above equation can be solved iteratively to find α_{OS} . The threshold is then calculated as:

$$T_{SO} = \alpha_{OS} * k^{th} sample \quad (4.20)$$

TM-CFAR

Gandhi and Kassam [17] have looked at the Trimmed Mean CFAR (TMCFAR) and they use a rank-ordered approach to estimate the mean interference power from a subset of samples. The subset of samples come from N reference cells and is a result of discarding N_{TL} largest samples and N_{TS} smallest samples. The mean of the subset is then used as the interference statistic. OS-CFAR and CACFAR are special cases of TM-CFAR with $(N_{TL}, N_{TS}) = (k - 1, N - k)$ and $(0,0)$ respectively. N_{TL} is a function of the number of interference targets to be eliminated and N_{TS} is for suppressing clutter edges. To address the problems of clutter edges and false alarms simultaneously, Gandhi suggests that for $N = 24$, let $N_{TL} = 18$ to 20 and $N_{TS} = 1$ to 3.

The expression for P_D and P_{FA} for TM CFAR are given by:

$$P_{D_{TM}} = \prod_{i=1}^{N-N_{TS}-N_{TL}} \gamma_i \left(\frac{\alpha_{TM}}{1 + SNR} \right) \quad (4.21)$$

and,

$$P_{FA_{TM}} = \prod_{i=1}^{N-N_{TS}-N_{TL}} \gamma_i(\alpha_{TM}) \quad (4.22)$$

where,

$$\gamma_1 = \frac{N!}{N_{TS}! (N - N_{TS} - 1)! (N - N_{TS} - N_{TL})} \sum_{k=0}^{N_{TL}} \frac{\binom{N_{TS}}{k} (-1)^{N_{TS}-k}}{N - k + \alpha_{TM}} \quad (4.23)$$

and,

$$\gamma_i = \frac{\frac{N - N_{TS} - i + 1}{N - N_{TS} - N_{TL} - i + 1}}{\frac{N - N_{TS} - i + 1}{N - N_{TS} - N_{TL} - i + 1} + \alpha_{TM}} \quad i = 2, 3, \dots, (N - N_{TS} - N_{TL}) \quad (4.24)$$

In this equation α_{TM} can be calculated using iterative means from equation 4.22. For this project, TMCFAR was not used for testing because iterative methods could not accurately find the exact value of α_{TM} and this lead to inconsistent results.

The following table shows a comparison made between various mentioned CFARs.

4.3.1.2.1.1 COMPARISON OF ALGORITHMS

	Environments			
CFAR	Homogeneou s	Interfering Targets	Clutter Boundaries	Interfering Targets and Clutter Boundaries
CA	x			
GO-CA			x	
SOCA		x		
OS		x	x	x
TM		x	x	x

The next section will look at the implementation of detection algorithms.

5 Implementation of CFAR

This chapter will look at the simulations carried out and their respective results. This is done to check if the implementation of different CFAR algorithms was correct.

To determine the probability of false alarm, CFAR algorithms were run on randomly generated noise from a standard normal distribution and the detections made were to determine P_{FA} . To calculate the probability of detection for each algorithm, a target was inserted.

The P_D and P_{FA} should be within 10% of the actual value for the implementation to be considered correct. The actual P_D value is calculated from the probability of detection equations in chapter 4.

5.1 CACFAR

Implementation

The CACFAR detector implementation was simulated using a $24 \times 1 * 10^6$ matrix as reference cells. The following values were used for the calculation:

$$N = 24, P_{FA} = 1 * 10^{-3} \text{ and SNR varying from 0 to } 30 \text{ dB.}$$

Verification

The resultant P_{FA} was less than 10%.

Using equation 4.5, the expected P_D was compared to the simulated and the results are shown below:

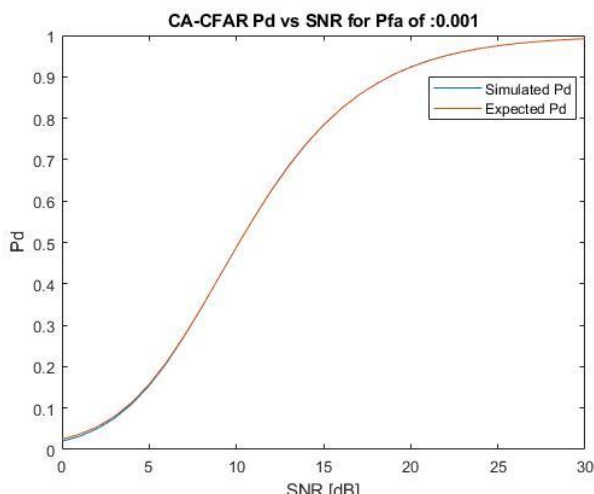


Figure 43: CACFAR Pd results

The implementation was confirmed to be correct since P_D and P_{FA} requirements were satisfied.

5.2 SOCACFAR

Implementation

The SOCACFAR detector implementation was simulated using a $24 \times 1 * 10^6$ matrix as reference cells. The following values were used for the calculation:

$N = 24$, $P_{FA} = 1 * 10^{-3}$ and SNR varying from 0 to 30 dB.

Verification

The resultant P_{FA} was less than 10%.

Using equation 4.15, the expected P_D was compared to the simulated and the results are shown below:

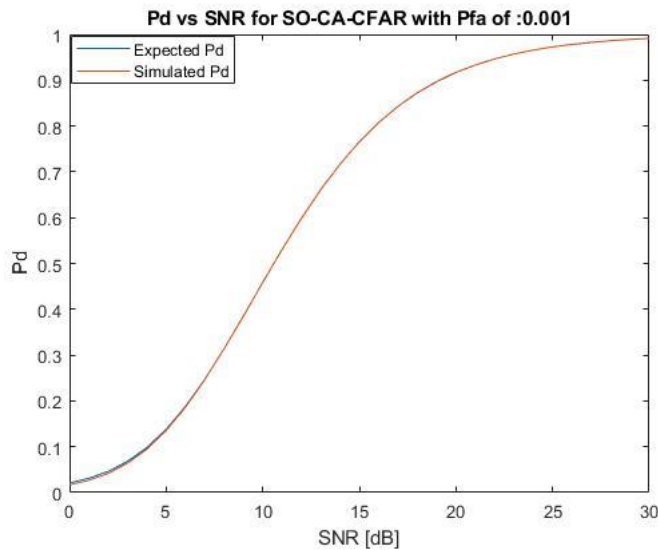


Figure 44: SOCACFAR Pd results

The implementation was confirmed to be correct since P_D and P_{FA} requirements were satisfied.

5.3 GOCACFAR

Implementation

The GOCACFAR detector implementation was simulated using a $24 \times 1 * 10^6$ matrix as reference cells. The following values were used for the calculation:

$$N = 24, P_{FA} = 1 * 10^{-3} \text{ and SNR varying from 0 to } 30 \text{ dB.}$$

Verification

The resultant P_{FA} was less than 10%.

Using equation 4.11, the expected P_D was compared to the simulated and the results are shown below:

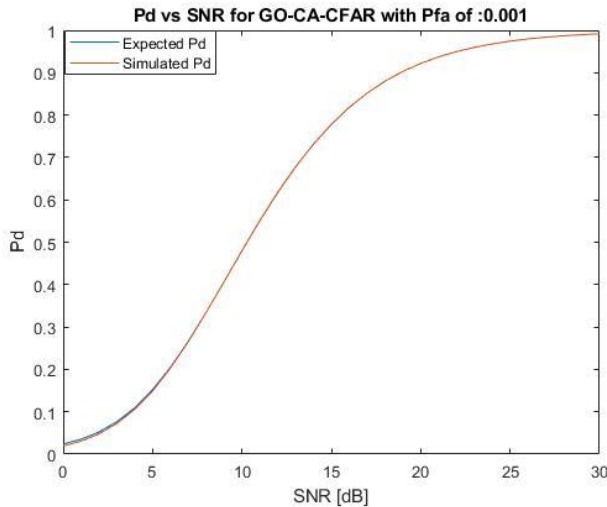


Figure 45: GOCACFAR Pd results

The implementation was confirmed to be correct since P_D and P_{FA} requirements were satisfied.

5.4 OSCFAR

Implementation

The CACFAR detector implementation was simulated using a $24 - by - 1 * 10^6$ matrix as reference cells. The following values were used for the calculation: $N = 24, P_{FA} = 1 * 10^{-3}$ and SNR varying from 0 to 30 dB.

Verification

The resultant P_{FA} was less than 10%.

Using equation 4.15, the expected P_D was compared to the simulated and the results are shown below:

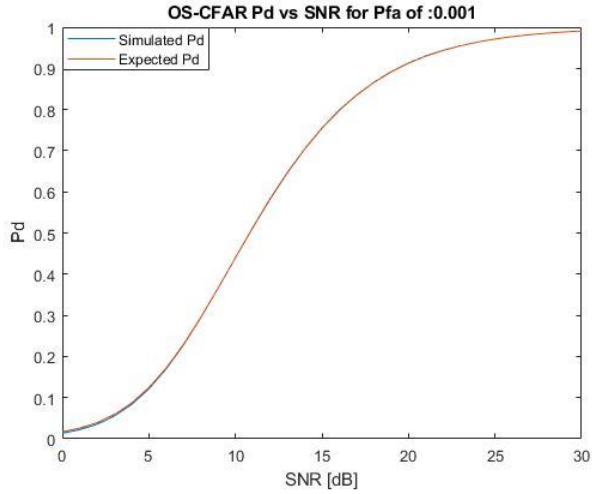


Figure 46: OSCFAR Pd results

The implementation was confirmed to be correct since P_D and P_{FA} requirements were satisfied.

The results showed that all CFAR implementations as the simulated values matched with the actual values for both P_D and P_{FA} . The next chapter will look at experiments and results.

6 Experiments and Results

This chapter will focus on the experiments carried out at the Sports Centre, Rugby Field and Cricket Field and the result collected.

6.1 Equipment

The following equipment was used to collect results

- S-Band radar, in FMCW mode.
- A Matlab GUI was created that processed the range data in the back-end and displayed the results on the screen. The App interface is shown below.

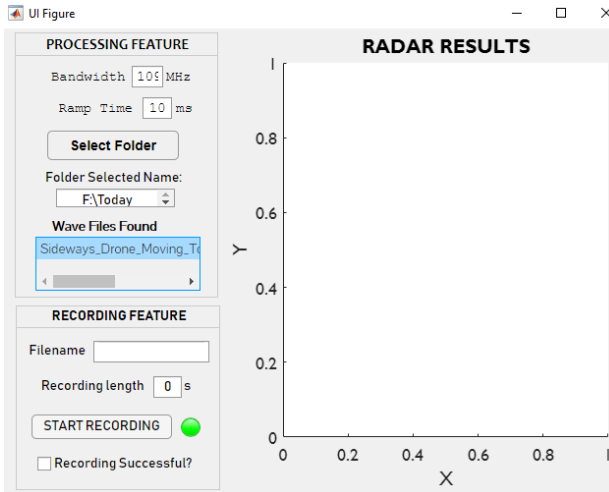


Figure 47: GUI interface

- A DJI Mavic Air drone was used for the experiment. Below, are the specifications of the drone

Table 3: Drone specifications

Weight	430 g
Dimensions unfolded	168×184×64 mm (L×W×H)
Dimensions folded	168×83×49 mm (L×W×H)
Max Speed	28.8 km/h
Battery Capacity and Voltage	2375 mAh
Operating Frequency	2.4-2.48 GHz; 5.7-5.8 GHz

6.2 Drone hazards

Before flying the drone, it was understood that drones fall under Remotely Piloted Aircraft Systems in the South African Civil Aviation Authority (SACCA) regulations [18]. Therefore, the following rules were observed in flying the drone

1. Not flying the drone 50 m or closer from Any person or a group of persons
2. Not flying the drone without the permission of the property owner

The following should not be done without permission from SACCA

1. Operation near manned aircrafts
2. Flying a drone weighing more than 7 kg
3. Flying in a prohibited airspace

To ensure the safety of other people was put first and to meet the SACCA regulations of flying a drone the following were done-

1. The drone was flown by an experienced drone pilot (Wian), and before each flight, the drone was inspected.
2. All the drone experiments were carried out in daylight and clear weather conditions.
3. The drone remained in the visual line of sight at all times.
4. The drone was flown in surrounding without people at all times.
5. Sports Centre managers were asked for permission before flying the drone.
6. The drone was flown in UCT which is away from other prohibited airspaces like those close to the Cape Town International Airport. No experiments were done near manned aircraft
7. The drone weighed 430g.

6.3 Clutter Modelling

Before performing any experiments, the clutter statistics of the environment have to be considered. Once the clutter statistics have been determined one can then apply a CFAR detector. In this project, the clutter statistics of the environment were not determined due to time constraints. Therefore, more work should be done to find the specific distribution for modelling the clutter statistics.

6.4 Radar Cross Section

The radar cross-section (RCS) is a measure of how detectable an object is or how much energy a target will reflect towards the radar. Therefore, the bigger the RCS, the more detectable an object. There are a number of factors that affect the RCS of an object and these include the size, material and shape of the object.

Size – bigger objects will provide a stronger radar reflection hence a higher RCS

Material – Highly reflective material will have a greater RCS than no-reflective objects of the same shape and size

Shape – Flat object will reflect more energy towards a radar than round or pointy objects hence higher RCS

RCS is relevant for this study because the drone is small and is mainly made of plastic. This might force developing solution to get a higher RCS.

6.5 MTI filtering

The algorithm for collecting range uses a Moving Target Indication (MTI) filtering. The filter is like a low pass filter that removes low-frequency signals. In doing so, only moving targets with a higher doppler frequency will be detected. The results of using an MTI are shown below:

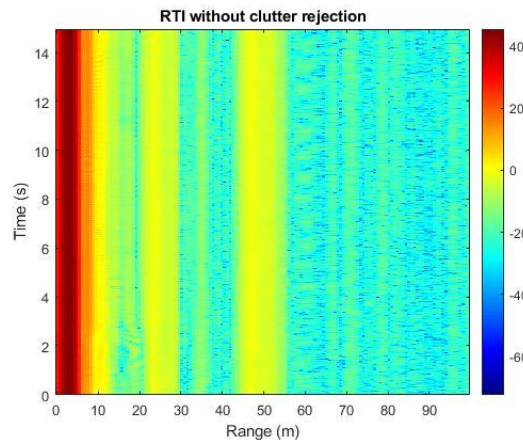


Figure 48: RTI map before MTI

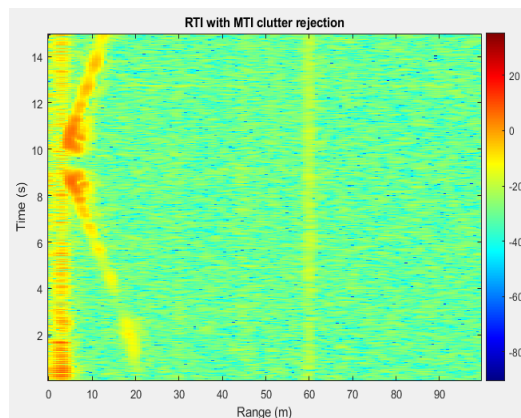


Figure 49: RTI map after MTI

6.6 Initial experiments and improvements

Initially, two drone orientations were tested, shown in Fig. 50 and 51, to find the best orientation for detection. The results showed that it was easier for the radar to pick up the drone with a side orientation (Fig. 52 and 53). The RCS was bigger, hence the results were better.

In the second set of experiments, the height at which the drone was flying was varied and the radar was positioned in such a way that it made a small angle with horizontal. The results were much better with the drone flying at a height of around 1.5 m above the radar (Fig. 54). It was decided that all drone experiments be carried out with the radar at an angle and the drone flying above the radar. The experiments were done at the Sports Centre.



Figure 50: Front section of a drone [19]



Figure 51: Side section of a drone [19]

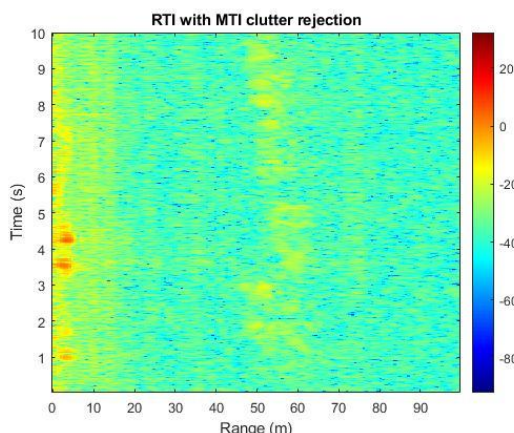


Figure 52: RTI map with drone front section

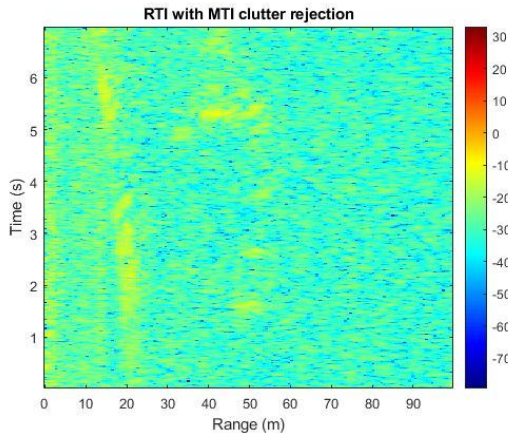


Figure 53: RTI map with a drone side section

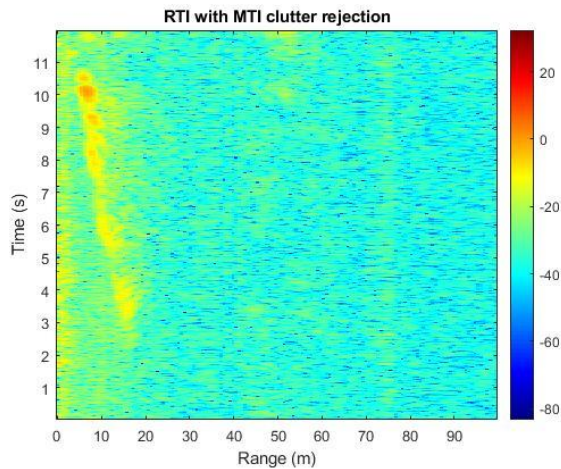


Figure 54: RTI map with a drone at a height of 1.5 above the radar with the radar at an angle

In the last experiments, a corner reflector was attached to the drone to improve the RCS. The results showed that the maximum detectable range of the radar improved (Fig. 57). The following pictures show the corner reflector and the radar readings taken.



Figure 55: Corner reflector before applying aluminium foil



Figure 56: Corner reflector after applying aluminium foil

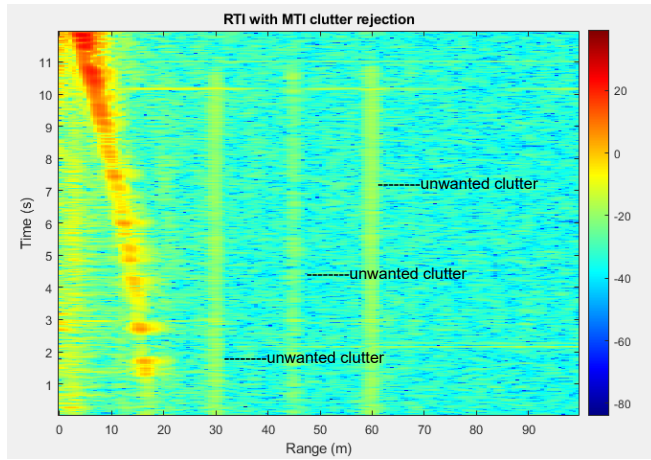


Figure 57: RTI map results with corner reflector

Experiment 1

This set of experiments were carried out at UCT Sports Center 2, Upper Campus. In these experiments, a reading was first taken without a target in the environment. The drone was flown away from the radar at the height of 2.5 m above the ground, starting from a horizontal distance of 4 m away from the radar and moving at an average speed of 1.25 m/s. The drone was flown until it was no detectable to the radar. Various results were taken and one (Fig. 60) was chosen for detection algorithm experiments.



Figure 58: Sports Centre setup

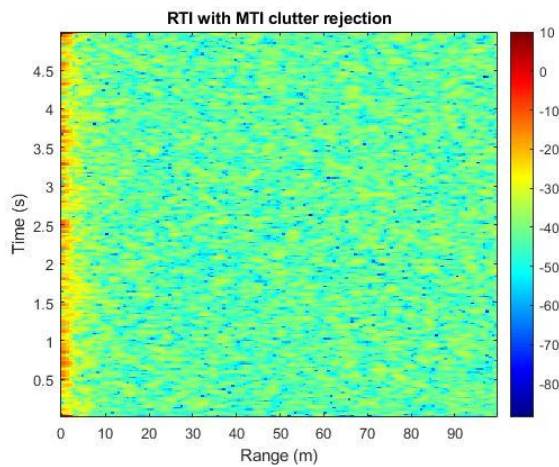


Figure 59: Noise only (no target)

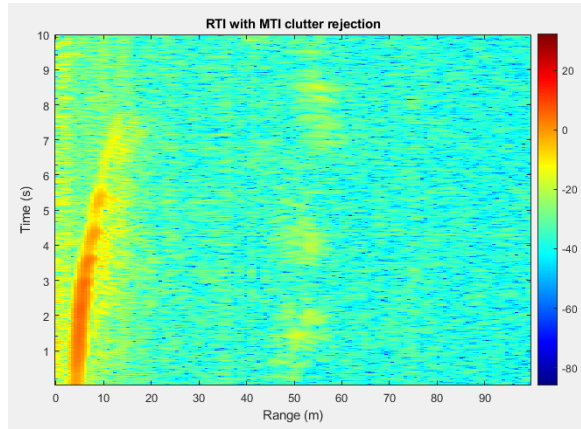


Figure 60: Drone moving away

Experiment 2

The second set of experiments were carried out at the UCT Rugby Field, Upper Campus. The wind speed was approximately 20 km/h as indicated from Google Weather. The following set of results were recorded:

1. Drone moving away, (starting distance = 4m, average speed = 1.5 m/s)
2. Drone moving away and then towards the radar (starting distance = 4 m, average speed = 2 m/s)
3. Drone moving towards and then away (starting distance = 22 m, average speed = 2 m/s)

Various results were collected, and the best results (Fig. 62-64) were selected for the detection algorithm experiments. The results are shown below:

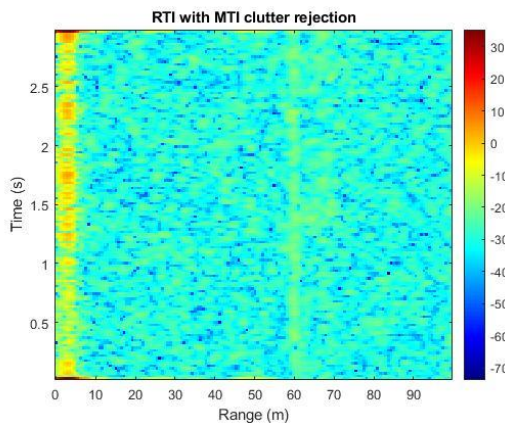


Figure 61: Noise only

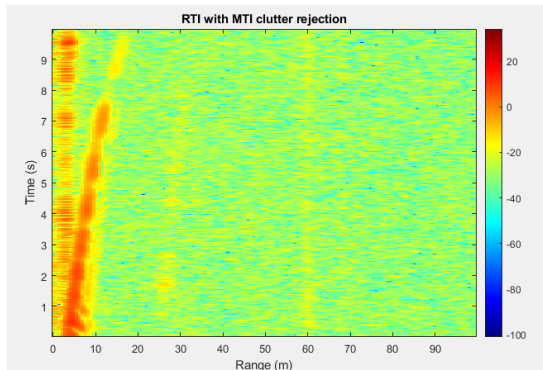


Figure 62: Drone moving away

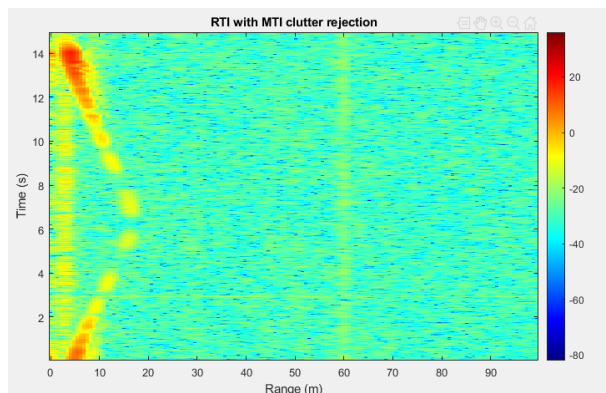


Figure 63: Drone moving away and then towards

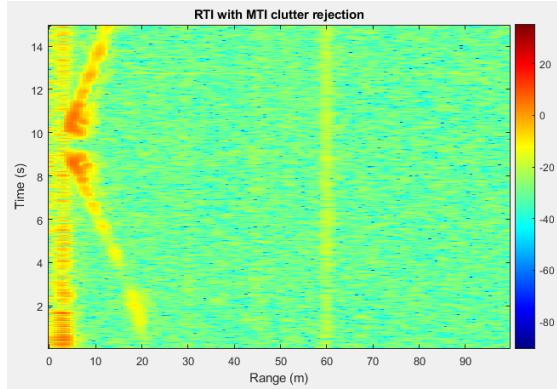


Figure 64: Drone moving towards and then away

Experiment 3

This set of experiments were carried out at UCT Cricket Field, Middle Campus. It was a calm day and with the wind speed was 6 km/h as reported by Google Weather. In these experiments, the drone was attached to a reflector

1. Drone flying away (starting distance = 4 m, average speed = 1.8 m/s)
2. Drone flying towards (starting distance = 22 m, average speed = 2.3 m/s)

The length of the string was 1 m. A long string was chosen so that the drone is minimally affected by random movements of the reflector because of the breeze.

The results were collected and the best results (Fig. 67 and 68) were chosen for detection algorithm experiments.



Figure 65: Cricket field setup

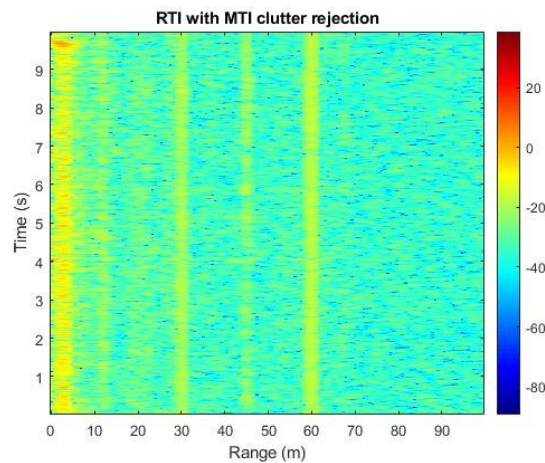


Figure 66: Noise only

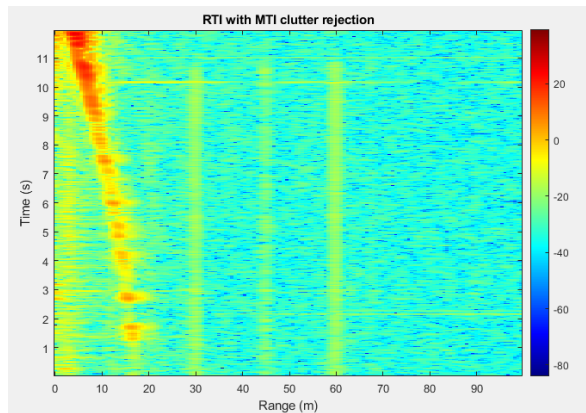


Figure 67: Drone moving towards

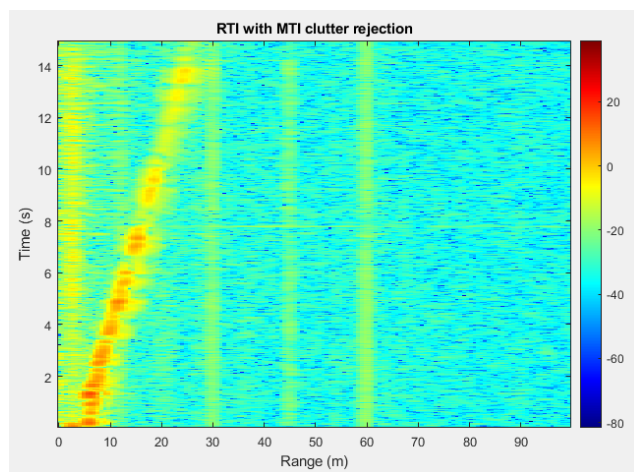


Figure 68: Drone moving away

7 CFAR Results

This Chapter will focus on collecting CFAR results from the results in the previous chapter.

7.1 Range Detection

CACFAR, GOCACFAR, SOCACFAR and OSCFAR were applied to the collected results from the previous chapter. The algorithms were written in such a way that where a detection is made, an ‘x’ will be placed over the range cell. The metric used for measuring the efficiency of each algorithm is the probability of detection over a specified range. The range of each detection algorithm was not used because, for the available data, the maximum range of each algorithm was insignificantly different from the others.

In the following diagrams $N = 32$, $P_{FA} = 1 * 10^{-8}$ and $G = 18$. P_{FA} was chosen to be this low to get rid of unwanted clutter readings. G was chosen to be 18 with 9 guard cells on each side. This value was chosen because G is a function of the maximum target extent and the maximum target extent was found to be 9 range cells.

The unwanted clutter might have been caused by a signal leaking from the circuit.

The following diagrams show the results from each experiment when OSCFAR was run. The results from other CFARs were very similar hence were not added.

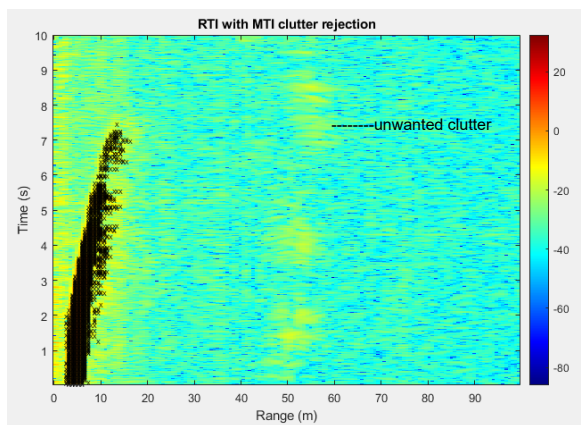


Figure 69: Final results from experiment 1

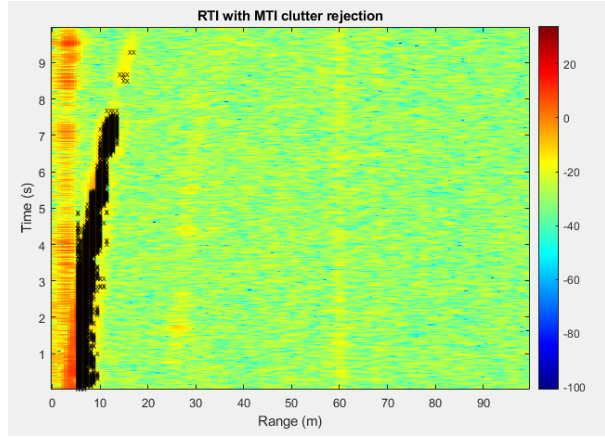


Figure 70: Final results from experiment 2.1

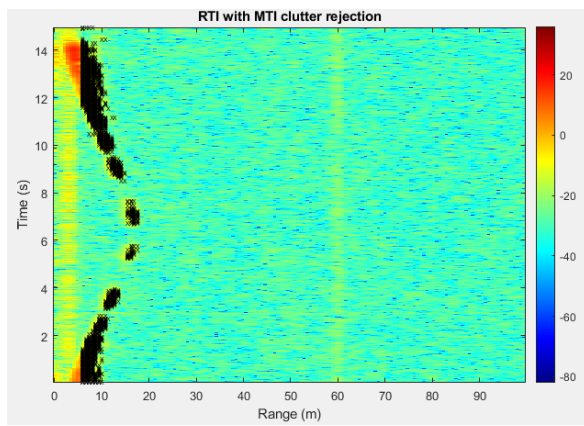


Figure 71: Final results from experiment 2.2

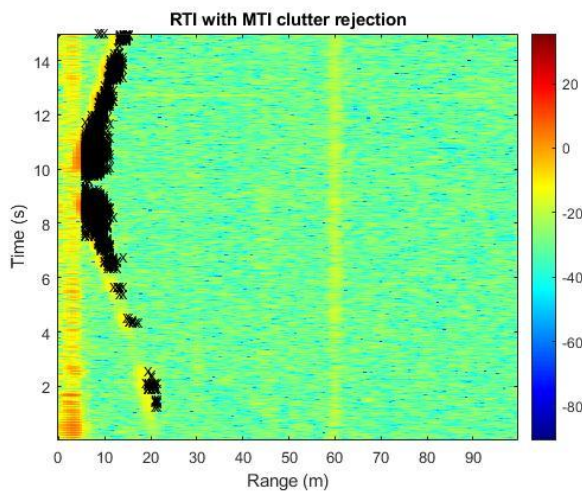


Figure 72: Final results from experiment 2.3

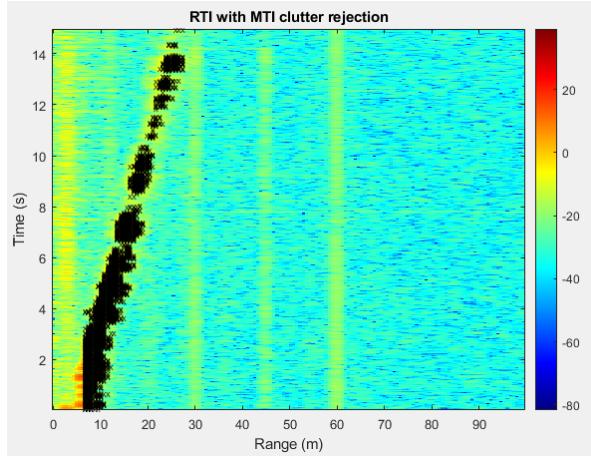


Figure 73: Final results from experiment 3.1

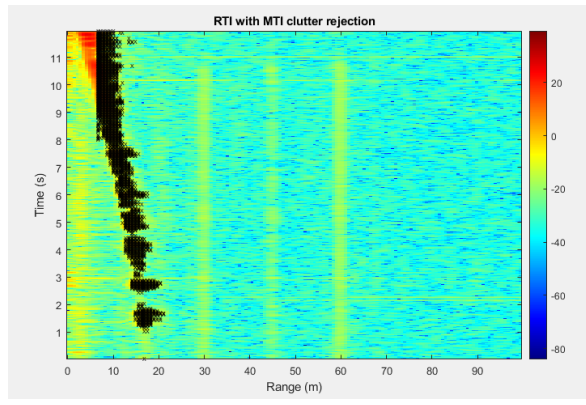


Figure 74: Final results from experiment 3.2

7.2 Probability of detection calculation

Calculating the probability of detection entails trying to identify the rows on the detection matrix that do not contain an 'x'. If an 'x' is not found in a row, then this will be regarded as a miss. If one 'x' or more are found in a row, then this will be regarded as a detection for that specific row. The probability of detection was calculated as the ratio of columns in which the detection is made to the number of columns over a user-defined region.

$$\text{Probability of detection} = \frac{\text{number of rows with an 'x'}}{\text{total number of rows}} * 100\% \quad (5.1)$$

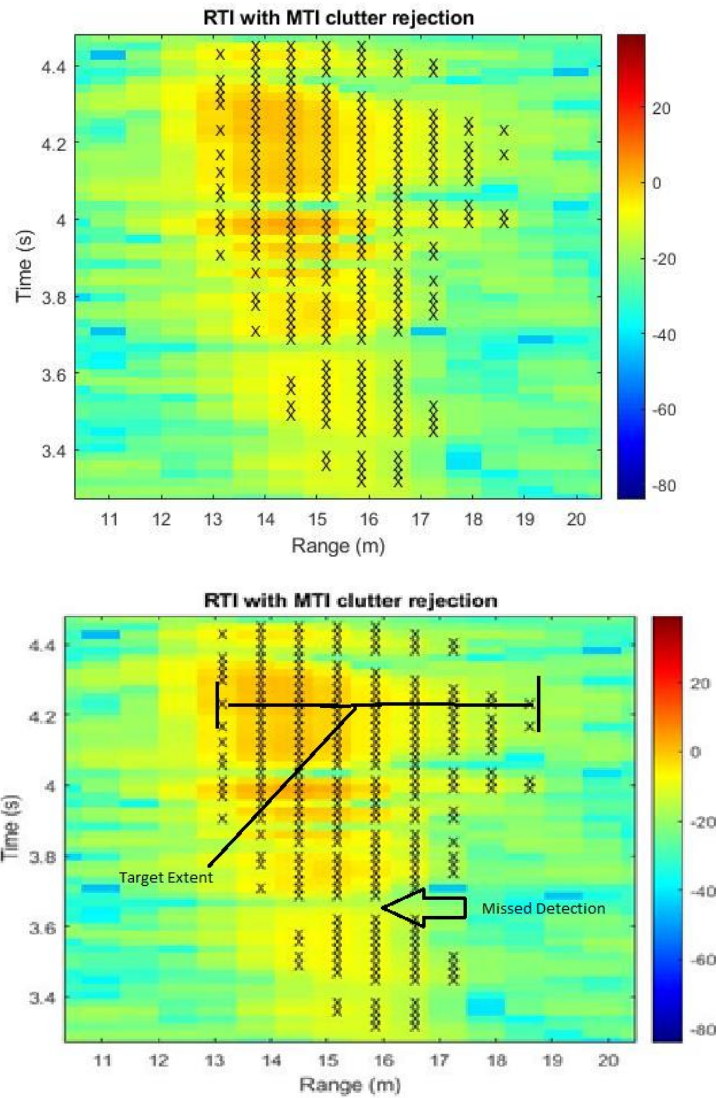


Figure 75: Picture showing a maximum target extent of 9 cells and missed detections

It is important to note that for experiment 1, the region of interest was between $0 < \text{time} < 8\text{s}$ while for the other experiments, the detection performance was measured for the whole time for which the drone readings were taken.

In presenting the results, the experiments were renamed as follows:

Table 4: Showing new experiment name

Old name	New name
Experiment 1	Experiment 1
Experiment 2.1	Experiment 2
Experiment 2.2	Experiment 3
Experiment 2.3	Experiment 4

Experiment 3.1	Experiment 5
Experiment 3.2	Experiment 6

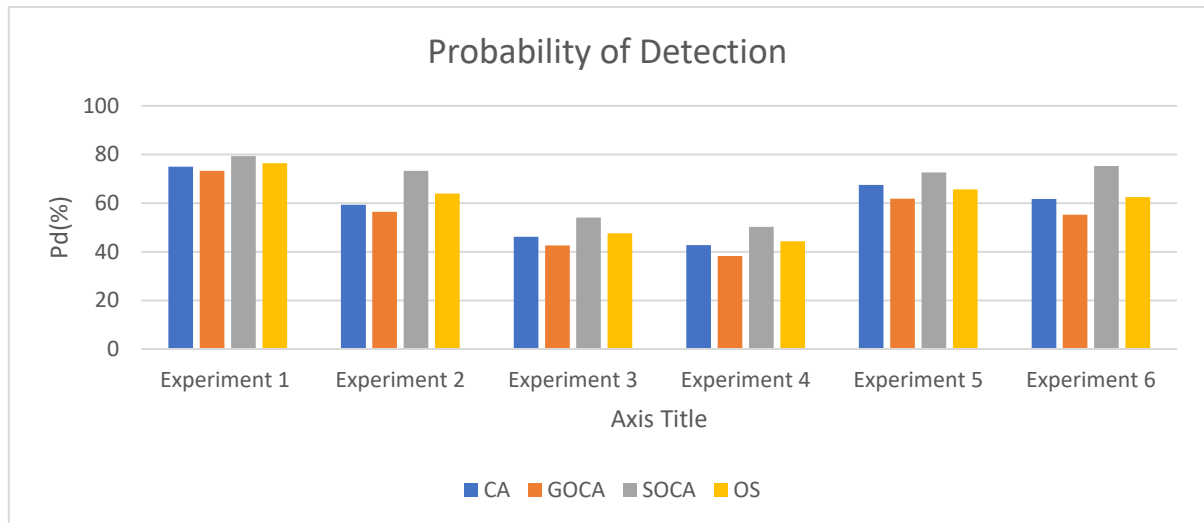
7.3 Result 1

The first set of results was produced using 16 reference cells ($N=16$), 8 lagging and 8 leading. The probability of false alarm was set at $1 * 10^{-8}$.

Table 5: Experiment results $N = 16$

	Exp 1	Exp 2	Exp 3	Exp 4	Exp 5	Exp 6
CA	75.00	59.30	46.13	42.71	67.54	61.75
GOCA	73.26	56.46	42.63	38.19	61.86	55.19
SOCA	79.36	73.30	54.01	50.29	72.63	75.23
OS	76.45	63.89	47.59	44.31	65.65	62.48

Table 6: Graphic results $N = 16$



Results summary

SOCACFAR performed better than all algorithms in every experiment. OSCFAR was second-best in all experiments except in experiment 5.

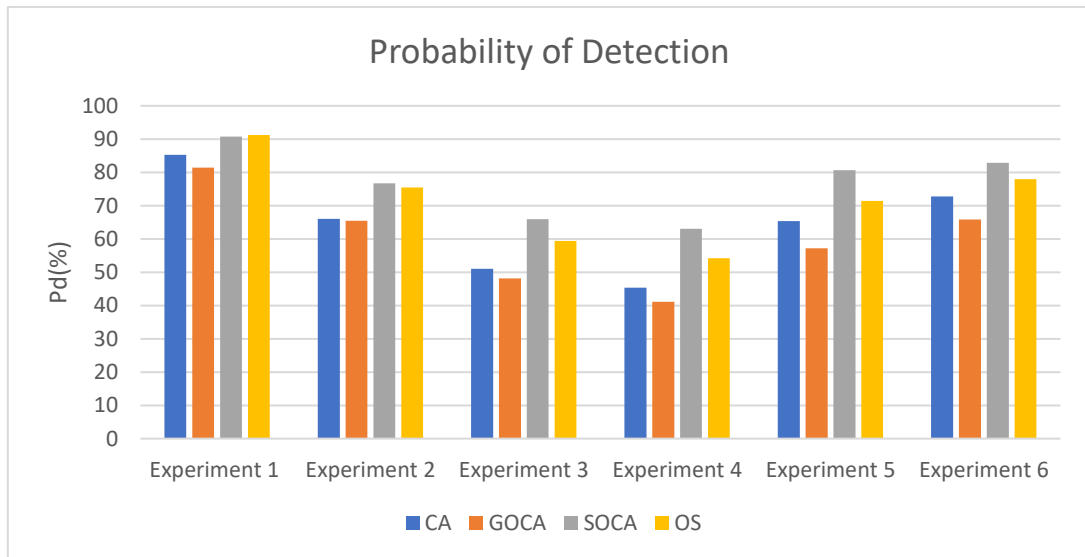
7.4 Result 2

The following set of results was produced with 32 reference cells($N=32$), 16 lagging and 16 leading. The probability of false alarm was set at $1 * 10^{-8}$.

Table 7: Results $N = 32$

	Exp 1	Exp 2	Exp 3	Exp 4	Exp 5	Exp 6
CA	85.29	66.01	51.02	45.40	65.32	72.76
GOCA	81.47	65.50	48.10	41.16	57.18	65.81
SOCA	90.74	76.75	65.94	63.07	80.70	82.90
OS	91.28	75.44	59.36	54.16	71.41	77.93

Table 8: Graphic results $N = 32$



Result Summary

The results show that SOCACFAR and OSCFAR performed consistently better than the other two algorithms.

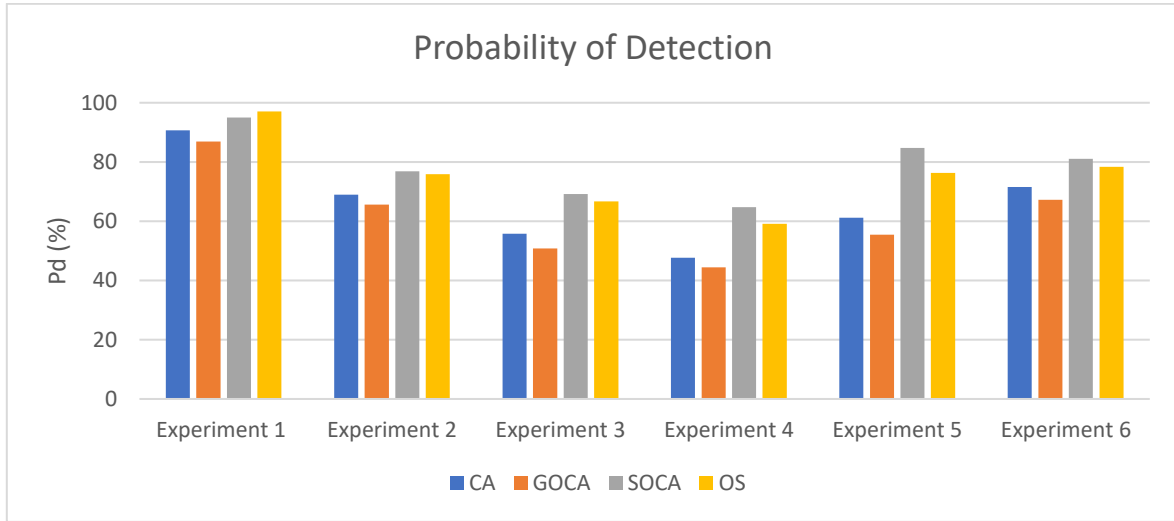
7.5 Result 3

This set of results was produced using 48 reference cells(N=48), 24 lagging and 24 leading. The probability of false alarm was set at $1 * 10^{-8}$.

Table 9: Experiment results N = 48

	Exp 1	Exp 2	Exp 3	Exp 4	Exp 5	Exp 6
CA	90.70	68.93	55.77	47.67	61.14	71.58
GOCA	86.92	65.65	50.80	44.46	55.46	67.21
SOCA	95.06	76.81	69.20	64.72	84.72	81.06
OS	97.09	75.93	66.72	59.18	76.27	78.32

Table 10: Graphic results N = 48



Result Summary

The results show that SOCACFAR and OSCFAR performed consistently better than the other two algorithms again.

8 Analysis of results

8.1 S-Band Radar Design

The constructed S-Band radar was able to detect the drone. The results were encouraging given that the drone was considerably small compared to other drones. Furthermore, the radar performed well despite the small cans used as antennas and the use of alternative components.

Despite various changes the changes made to the original MIT radar, the radar was able to meet the design specifications. As a result, it was learnt that when designing a circuit following steps outlined in a document, one does not always need to use the suggested components especially if they are costly. Cheaper alternatives that can serve the same function should be searched for before committing resources.

8.2 Probability of Detection

The results show that SOCACFAR and OSCFAR performed consistently better than other algorithms. In homogeneous environments, CACFAR is expected to perform better than other algorithms [17]. The results may suggest that the environment was not homogeneous. Amongst the two best algorithms, SOCACFAR is expected to perform very well in environments where there are multiple targets while OSCFAR is able to tackle environments that might have clutter edges and interfering targets.

Using a corner reflector significantly improved the detection range up to about 30 m from 20 m. The use of a reflector improved the RCS since aluminium foil is a highly reflective material.

From the results graphs, there is a dip in experiment 3 and 4. This is because, in these experiments, the drone would stop moving as it changes the direction of motion. As a result, the returns were killed by the MTI filter leaving more times with missing detections.

Increasing the number of reference cells resulted in an overall increase in the probability of detection. This is consistent with detection theory since a bigger number of reference

cells will ensure that more cells are taken into account when estimating the interference statistics. As a result, threshold value will be more accurately determined leading to better results. It is important to note that the number of reference cells can be made as large as possible for CACFAR as long as the reference cells do not contain interfering targets. OSCFAR and SOCACFAR will suppress a limited number of interfering targets in reference cells and this used to determine the N value.

The results showed that SOCACFAR and OSCFAR performed consistently better than other CFARs. However, the CFAR results of the two algorithms were very close. It is then necessary to consider other advantages of the two CFARs. OSCFAR has numerous advantages that SOCACFAR does not have. OSCFAR can tackle the problem of interfering targets and clutter boundaries, at the same time, while SOCACFAR succumbs to clutter boundaries.

Furthermore, OSCFAR allows the user to set the maximum number of interfering targets that can be suppressed and can also suppress interfering targets in either the leading or lagging cells. SOCACFAR is limited in both of these areas. It cannot suppress interfering targets in leading and lagging cells at the same time and the maximum number of suppressed targets cannot be set. There is, therefore, more flexibility in using OSCFAR. Given these advantages, OSCFAR will perform much better in the presence of numerous drones and clutter boundaries. Hence, SOCACFAR is the best detection algorithm for the detection of drones amongst the four algorithms.

9 Conclusions and Recommendations

9.1 Conclusions

Building a working S-Band radar was done successfully using the understanding from FMCW and CW theory. Hence, objectives 1 and 2 were successfully met.

In the detection theory section, CACFAR, GOCACFAR, OSCFAR, SOCACFAR and TMCFAR were looked at, in greater detail. Furthermore, implementations of the first 4 CFARs were used to calculate the probability of detection on the results from the main experiments. In doing this, objectives 4 and 5 were fully met.

Finally, OSCFAR was proposed as the detection algorithm of choice because of its ability to operate effectively in different environments and the flexibility associated with choosing the number of targets that can be suppressed. Therefore, objective 5 was fully met.

Using this evaluation, the project was considered a success. However, there are ways that the project can be improved or extended, and these will be covered in the next section.

9.2 Recommendations

For this project, more research should be done on modelling the clutter characteristics for associated with environments in which experiments will be done. Such work is important in order to be able to confidently use CFAR algorithms for drone detection.

Secondly, combining various CFARs to come up with an adaptive CFAR would be interesting to look at. This approach has been used in [20].

Future research can also look at the use of micro-doppler signatures of drones for classification. This is very important because drones can be easily mistaken with birds which would lead to an increase in false alarms in the system.

10 References

- [1] N. Kozhanov, The attacks on Aramco could hurt Saudi Arabia in the long term, AlJAZEERA, 2019.
- [2] W. Hennigan, “Experts Say Drones Pose a National Security Threat — and We Aren’t Ready,” Time, 31 May 2018. [Online]. Available: <https://time.com/5295586/drones-threat/>. [Accessed 14 October 2019].
- [3] G. Charvat, J. Williams, F. A, K. S and H. J, “MIT OpenCourseWare,” Massachusetts Institute of Technology, January 2011. [Online]. Available: <https://ocw.mit.edu>. [Accessed October 2019].
- [4] S. Jeon, J. Shin, Y. Lee, W. Kim, Y. Kwon and H. Yang, “Empirical study of drone sound detection in real-life environment with deep neural networks,” in *25th European Signal Processing Conference (EUSIPCO) 2017*, 2017.
- [5] R. Mohammad, T. Hamid, H. Mahdi and K. SS., “A NEW FRAMEWORK FOR DETECTING AND TRACKING DRONES,” *Indian Journal of Fundamental and Applied Life Sciences*, vol. 4, no. S4, p. 2231– 6345, 2014.
- [6] M. Ezuma, O. Ozdemir, C. Anjinappa, W. Gulzar and G. I., “Micro-UAV detection with a low-grazing angle millimeter wave radar.,” in *Aerospace Conference 2019*, 2019.
- [7] M. Jian, Z. Lu and V. Chen, “Drone Detection and Tracking Based on Phase-Interferometric Doppler Radar,” p. 4, 2018.
- [8] X. Yang, K. Huo, W. Jiang, J. Zhao and Q. Z, “passive radar system for detecting UAV based on the OFDM communication signal,” in *Progress in Electromagnetic Research Symposium (PIERS)*, 2016.
- [9] G. Rehm, “How To Build A Tin Can Waveguide WiFi Antenna,” Turnpoint, 2003-2007. [Online]. Available: <https://www.turnpoint.net/wireless/cantennahowto.html>. [Accessed 14 October 2019].
- [10] RS Components, “RS,” 2019. [Online]. Available: <https://docs-emea.rs-online.com/webdocs/1588/0900766b81588686.pdf>. [Accessed 14 October 2019].

- [11] Minicircuits, "Voltage Controlled Oscillator," Minicircuits, 2019. [Online]. Available:
] <https://www.minicircuits.com/pdfs/ZX95-2536C+.pdf>. [Accessed 15 October 2019].
- [12] M. Pichards, A. Scheer JA and W. Holm, Principles of Modern Radar, vol. 1,
] Raleigh: SciTech Publishing, 2010, pp. 604-611.
- [13] V. Hansen and J. Sawyers, "Detectability Loss Due to "Greatest Of" Selection in a
] Cell-Averaging CFAR," *IEEE Transactions on Aerospace and Electronic Systems*,
 Vols. AES-16, no. 1, pp. 115-118, 1980.
- [14] G. Trunk, "Range resolution of targets using automatic detectors," *IEEE*
] *Transactions on Aerospace and Electronic Systems*, Vols. AES-14, no. 5, pp. 750-
 755, 1978.
- [15] H. Rohling, "New CFAR-processor based on an ordered statistic," in *International*
] *Radar Conference*, Arlington, 1985.
- [16] H. Rohling, "Radar CFAR Thresholding in Clutter and Multiple Target Situations,"
] *IEEE Transactions on Aerospace and Electronic Systems*, Vols. AES-19, no. 4, pp.
 608-621, 1993.
- [17] P. Gandhi and S. Kassam, "Analysis of CFAR processors in nonhomogeneous
] background," *IEEE Transactions on Aerospace and Electronic Systems*, vol. 24, no.
 4, pp. 427- 445, 1998.
- [18] South African Civil Aviation Authority, "Remotely Piloted Aircraft Systems," South
] African Civil Aviation Authority, 2017. [Online]. Available:
<http://wwwcaa.co.za/Pages/RPAS/Remotely%20Piloted%20Aircraft%20Systems.aspx>. [Accessed 2019].
- [19] Visual Aerials, "VA static images," Visual Aerials, [Online]. Available:
] <http://visual-aerials.com/mavicpro.html>. [Accessed 14 October 2019].
- [20] D. Ivković, M. Andrić and B. Zrnić, "Detection of very close targets by fusion CFAR
] detectors," *Scientific Technical Review*, vol. 66, no. 3, pp. 50-57, 2016.
- [21] P. Gandhi and S. Kassam, "Analysis of CFAR processors in nonhomogeneous
] background," *IEEE Transactions on Aerospace and Electronic systems*, vol. 24, no.
 4, pp. 427-445, 1988.

11 Appendices

Rugby Field Results

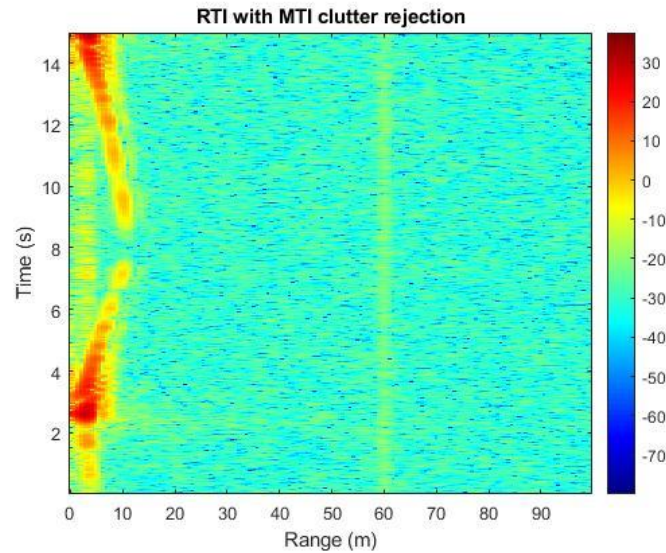


Figure 76: Drone moving away and towards

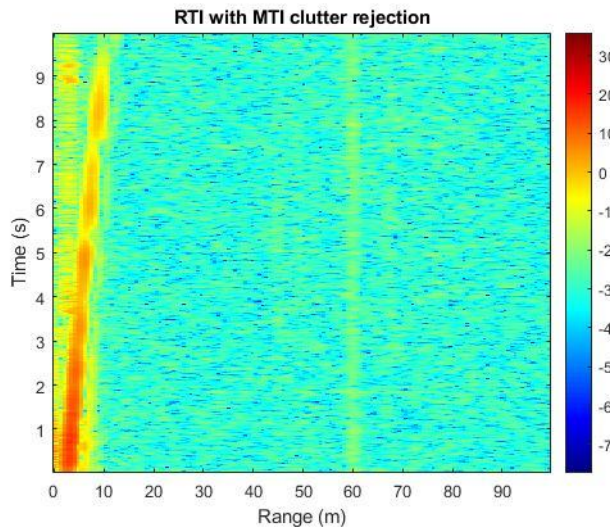


Figure 77: Drone moving away slowly

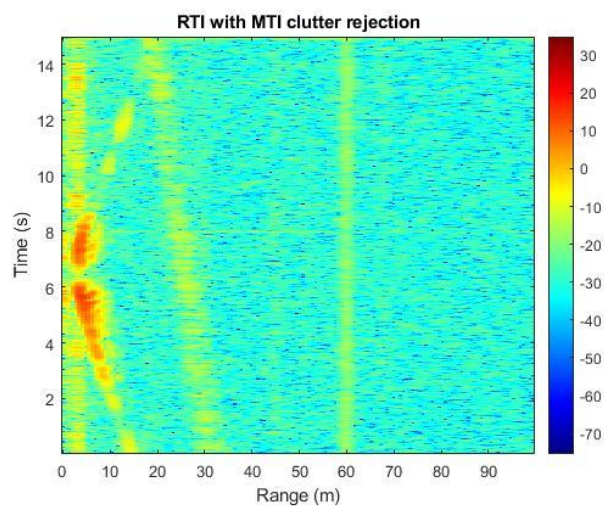


Figure 78: drone flying towards and away

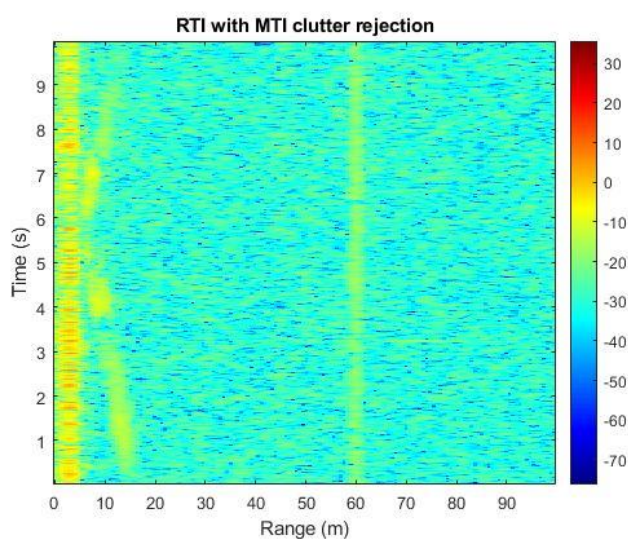


Figure 79: Drone flying cross range

Cricket Field

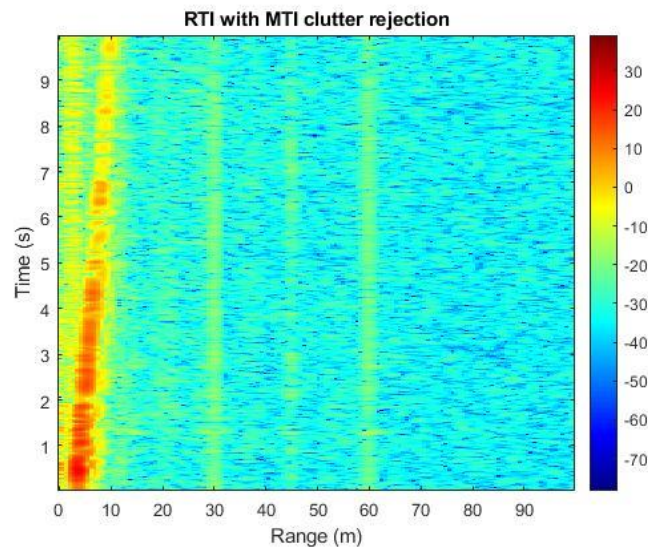


Figure 80: Drone flying away slowly

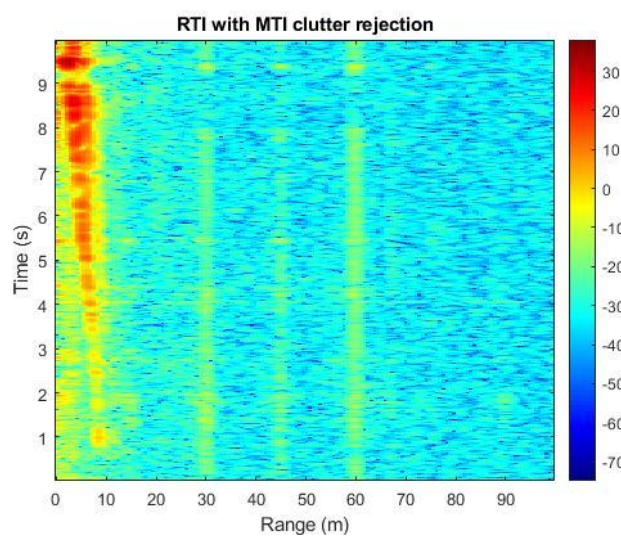


Figure 81: Drone flying towards

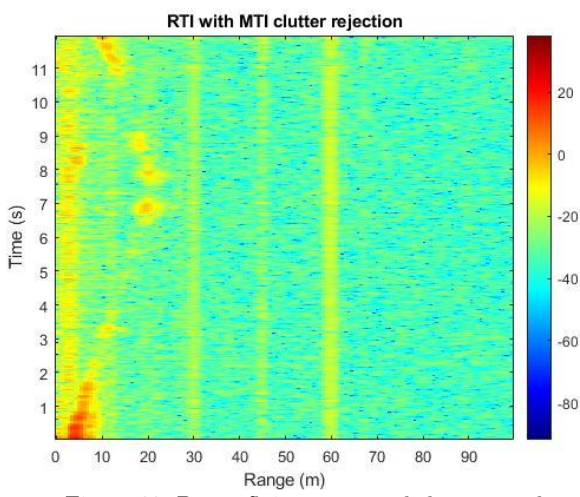


Figure 82: Drone flying away and then towards

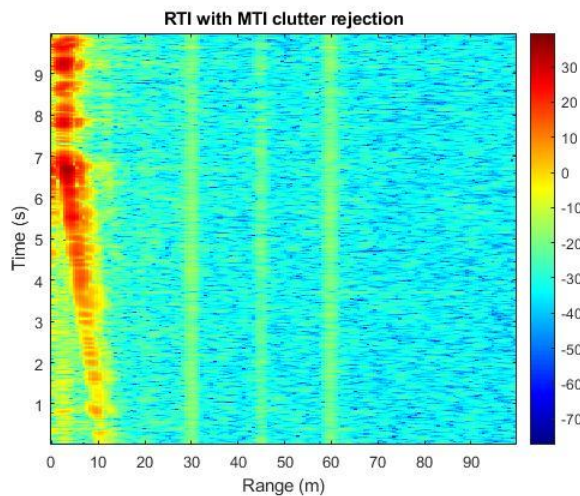


Figure 83: Drone flying towards

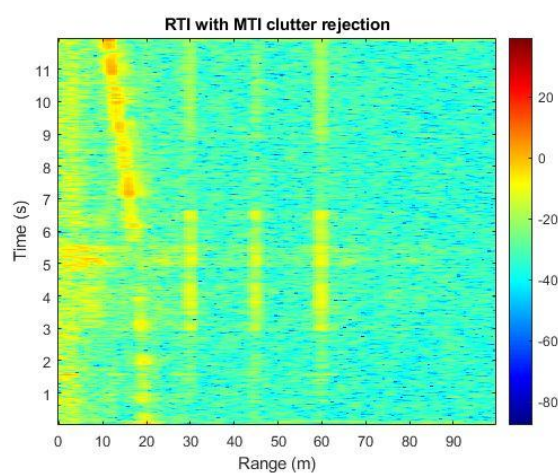


Figure 84: Drone flying towards

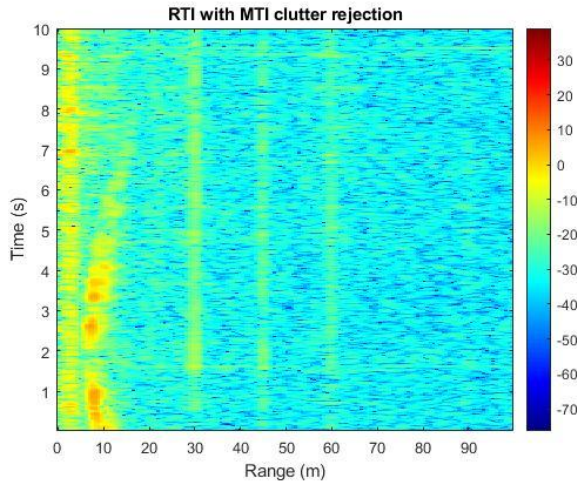


Figure 85: Drone flying cross range

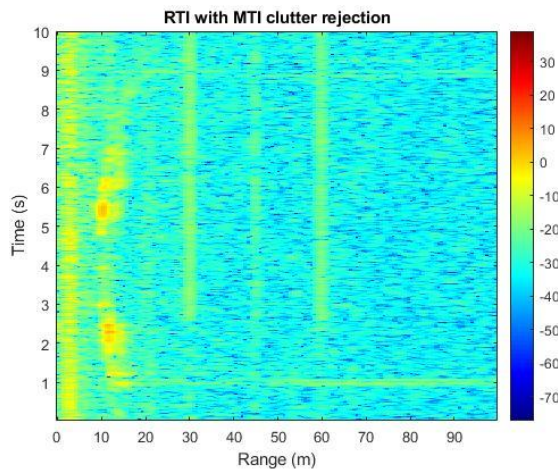


Figure 86: Drone flying cross range

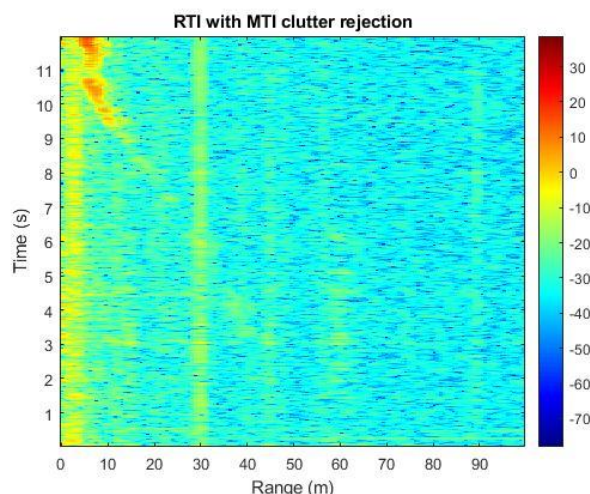


Figure 87: Drone flying towards

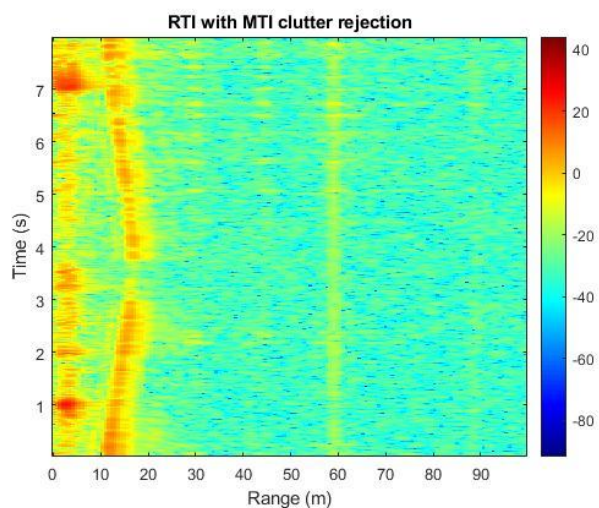


Figure 88: Drone flying away and towards

TEST4

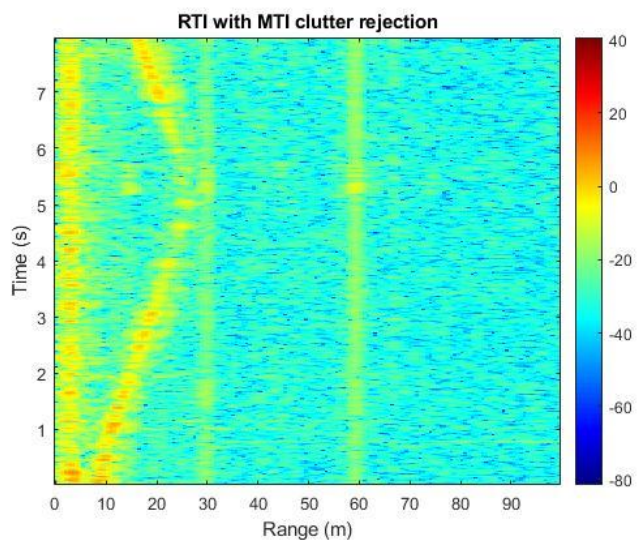


Figure 89: Drone flying away and towards

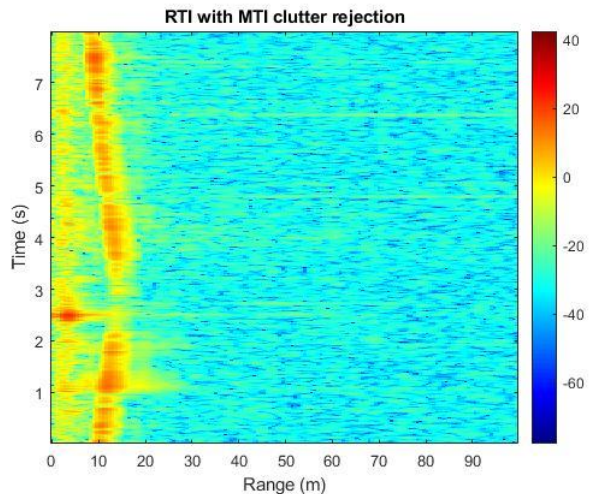


Figure 90: Drone flying away and towards

Sports Centre Results

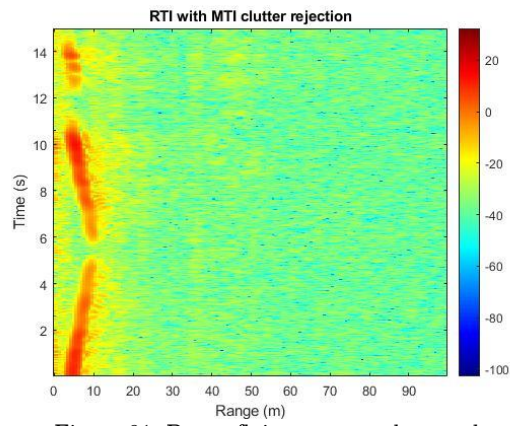


Figure 91: Drone flying away and towards

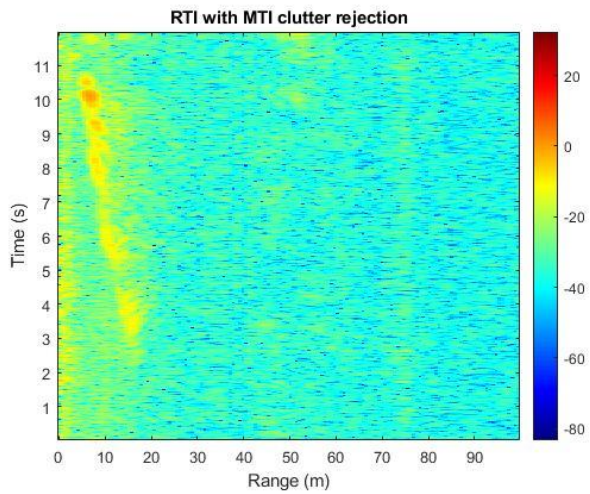


Figure 92: Drone flying towards

12 EBE Faculty: Assessment of Ethics in Research Projects

Any person planning to undertake research in the Faculty of Engineering and the Built Environment at the University of Cape Town is required to complete this form before collecting or analysing data. When completed it should be submitted to the supervisor (where applicable) and from there to the Head of Department. If any of the questions below have been answered YES, and the applicant is NOT a fourth year student, the Head should forward this form for approval by the Faculty EIR committee: submit to Ms Zulpha Geyer (Zulpha.Geyer@uct.ac.za; Chem Eng Building, Ph 021 650 4791). Students must include a copy of the completed form with the final year project when it is submitted for examination.

Name of Principal		
Researcher/Student:	NYASHA MASHANDA	
Department:	ELECTRICAL ENGINEERING	
If a Student: YES	Degree: Electrical	Supervisor: Dr Yunus Abdul Gaffar
If a Research Contract indicate source of funding/sponsorship:		No
Research Project		
Title:	Radar Detection of a drone using a S-Band Radar	

Overview of ethics issues in your research project:

Question 1: Is there a possibility that your research could cause harm to a third party (i.e. a person not involved in your project)?	YES	NO <input checked="" type="checkbox"/>
Question 2: Is your research making use of human subjects as sources of data? If your answer is YES, please complete Addendum 2.	YES	NO <input checked="" type="checkbox"/>
Question 3: Does your research involve the participation of or provision of services to communities? If your answer is YES, please complete Addendum 3.	YES	NO <input checked="" type="checkbox"/>
Question 4: If your research is sponsored, is there any potential for conflicts of interest? If your answer is YES, please complete Addendum 4.	YES	NO <input checked="" type="checkbox"/>

If you have answered YES to any of the above questions, please append a copy of your research proposal, as well as any interview schedules or questionnaires (Addendum 1) and please complete further addenda as appropriate.

I hereby undertake to carry out my research in such a way that

- there is no apparent legal objection to the nature or the method of research; and
- the research will not compromise staff or students or the other responsibilities of the University;
- the stated objective will be achieved, and the findings will have a high degree of validity;
- limitations and alternative interpretations will be considered;
- the findings could be subject to peer review and publicly available; and
- I will comply with the conventions of copyright and avoid any practice that would constitute plagiarism.

Signed by:

	Full name and signature	Date
Principal Researcher/Student:	Nyasha Mashanda	15 October 2019

This application is approved by:

Supervisor (if applicable):	Dr Yunus Abdul Gaffar	15 October 2019
-----------------------------	-----------------------	-----------------

HOD (or delegated nominee): Final authority for all assessments with NO to all questions and for all undergraduate research.	Janine Buxey	15 October 2019
Chair : Faculty EIR Committee For applicants other than undergraduate students who have answered YES to any of the		

ADDENDUM 1:

Please append a copy of the research proposal here, as well as any interview schedules or questionnaires:

ADDENDUM 2: To be completed if you answered YES to Question 2:

It is assumed that you have read the UCT Code for Research involving Human Subjects (available at <http://web.uct.ac.za/depts/educate/download/uctcodeforresearchinvolvinghumansubjects.pdf>) in order to be able to answer the questions in this addendum.

2.1 Does the research discriminate against participation by individuals, or differentiate between participants, on the grounds of gender, race or ethnic group, age range, religion, income, handicap, illness or any similar classification?	YES	NO
2.2 Does the research require the participation of socially or physically vulnerable people (children, aged, disabled, etc) or legally restricted groups?	YES	NO
2.3 Will you not be able to secure the informed consent of all participants in the research? (In the case of children, will you not be able to obtain the consent of their guardians or parents?)	YES	NO
2.4 Will any confidential data be collected or will identifiable records of individuals be kept?	YES	NO
2.5 In reporting on this research is there any possibility that you will not be able to keep the identities of the individuals involved anonymous?	YES	NO
2.6 Are there any foreseeable risks of physical, psychological or social harm to participants that might occur in the course of the research?	YES	NO
2.7 Does the research include making payments or giving gifts to any participants?	YES	NO

If you have answered YES to any of these questions, please describe below how you plan to address these issues:

ADDENDUM 3: To be completed if you answered YES to Question 3:

3.1 Is the community expected to make decisions for, during or based on the research?	YES	NO
3.2 At the end of the research will any economic or social process be terminated or left unsupported, or equipment or facilities used in the research be recovered from the participants or community?	YES	NO
3.3 Will any service be provided at a level below the generally accepted standards?	YES	NO

If you have answered YES to any of these questions, please describe below how you plan to address these issues:

ADDENDUM 4: To be completed if you answered YES to Question 4

4.1 Is there any existing or potential conflict of interest between a research sponsor, academic supervisor, other researchers or participants?	YES	NO
4.2 Will information that reveals the identity of participants be supplied to a research sponsor, other than with the permission of the individuals?	YES	NO
4.3 Does the proposed research potentially conflict with the research of any other individual or group within the University?	YES	NO

If you have answered YES to any of these questions, please describe below how you plan to address these issues: